Published in final edited form as:

*Cell Rep*. 2021 May 18; 35(7): 109134. doi:10.1016/j.celrep.2021.109134.

# Axonal generation of amyloid-β from palmitoylated APP in mitochondria-associated endoplasmic reticulum membranes

**Raja Bhattacharyya**[1,*], **Sophia E. Black**[1], **Madhura S. Lotlikar**[1], **Rebecca H. Fenn**[1], **Mehdi Jorfi**[1], **Dora M. Kovacs**[1], **Rudolph E. Tanzi**[1,2,*]

[1]Genetics and Aging Research Unit, MassGeneral Institute for Neurodegenerative Disease, Henry and Allison McCance Center for Brain Health, Department of Neurology, Massachusetts General Hospital, Harvard Medical School, Boston, MA, USA

[2]Lead contact

## SUMMARY

Axonal generation of Alzheimer's disease (AD)-associated amyloid-β (Aβ) plays a key role in AD neuropathology, but the cellular mechanisms involved in its release have remained elusive. We previously reported that palmitoylated APP (*pal*APP) partitions to lipid rafts where it serves as a preferred substrate for β-secretase. Mitochondria-associated endoplasmic reticulum (ER) membranes (MAMs) are cholesterol-rich lipid rafts that are upregulated in AD. Here, we show that downregulating MAM assembly by either RNA silencing or pharmacological modulation of the MAM-resident sigma1 receptor (S1R) leads to attenuated β-secretase cleavage of *pal*APP. Upregulation of MAMs promotes trafficking of *pal*APP to the cell surface, β-secretase cleavage, and Aβ generation. We develop a microfluidic device and use it to show that MAM levels alter Aβ generation specifically in neuronal processes and axons, but not in cell bodies. These data suggest therapeutic strategies for reducing axonal release of Aβ and attenuating β-amyloid pathology in AD.

## In brief



*Correspondence: bhattacharyya.raja@mgh.harvard.edu (R.B.), tanzi@helix.mgh.harvard.edu (R.E.T.).

AUTHOR CONTRIBUTIONS

R.B. and R.E.T. conceived the study, analyzed the data, supervised the study, and wrote the manuscript. R.B., S.E.B., M.S.L., and R.H.F. performed the experiments. M.J. contributed in designing in-house microfluidic chambers. D.M.K. provided valued insights and contributed in manuscript writing.

DECLARATION OF INTERESTS

R.E.T. and D.M.K. hold intellectual property and patents on the topic of acyl-CoA:cholesterol acyltransferase inhibitors (patent no. US20050118226A1) and methods and compositions relating to modulating amyloid precursor protein cleavage (patent no. US20050170437A1).

INCLUSION AND DIVERSITY

We worked to ensure sex balance in the selection of non-human subjects. We worked to ensure diversity in experimental samples through the selection of the cell lines. We worked to ensure diversity in experimental samples through the selection of the genomic datasets.

SUPPLEMENTAL INFORMATION

Supplemental information can be found online at https://doi.org/10.1016/j.celrep.2021.109134.

Bhattacharyya et al. show that the modulation of mitochondrial-associated endoplasmic reticulum membranes (MAMs) via sigma-1 receptor regulates Aβ generation from axons via cell surface trafficking and β-secretase cleavage of MAM-resident palmitoylated APP (*pal*APP).

## Graphical Abstract

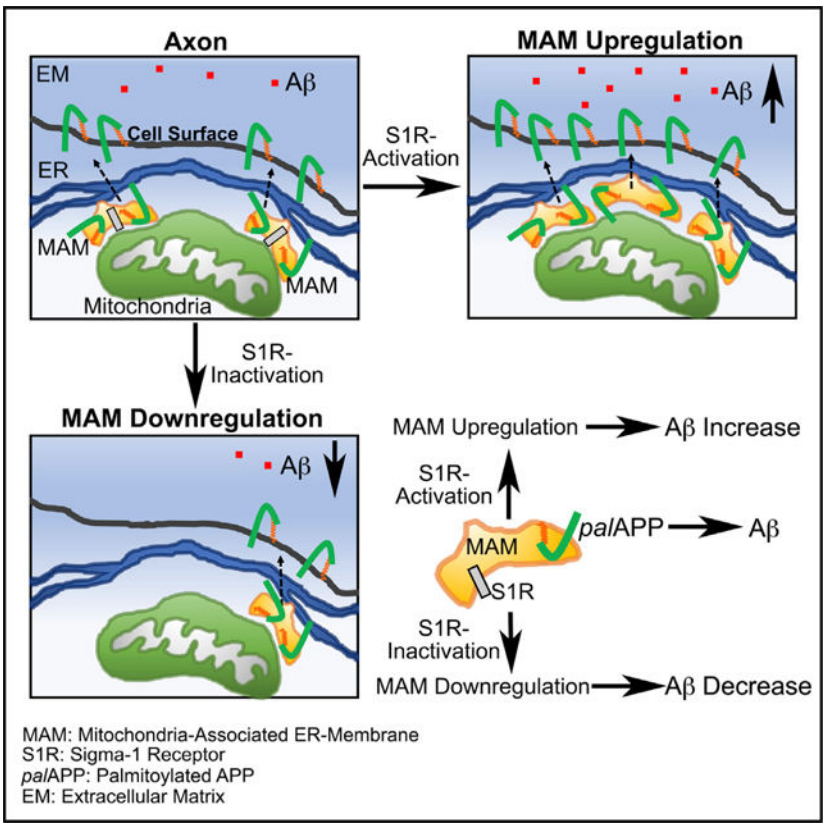


## INTRODUCTION

The subcellular localization of amyloid-β (Aβ) generation and downstream effects on neurons are key events in Alzheimer's disease (AD) neuropathogenesis (Simons 1995; Yamazaki et al., 1995; Koo et al., 1996; Muresan et al., 2009). Synaptic and neuritic Aβ can be generated via processing of APP in neuronal processes (Kamal et al., 2001; Cirrito et al., 2008; Tampellini et al., 2009; Das et al., 2013), ~40% of neuronal Aβ production takes place in axons (Niederst et al., 2015; Das et al., 2016). However, the molecular mechanisms underlying axonal generation of Aβ remain elusive.

To transport proteins to the cell surface, axons use endoplasmic reticulum (ER)-rafts or mitochondria-associated ER membranes (MAMs), found on the ER juxtaposed with mitochondria (Merianda et al., 2009). 5%–20% of the mitochondrial surface associates with the ER to form MAMs (Hajnóczky et al., 2006; Rowland and Voeltz, 2012). MAMs move bidirectionally as isolated small ER (sER) vesicles in neuronal processes (Pizzo and Pozzan, 2007; Giorgi et al., 2009). Mitochondria are essential for the formation and maintenance of

synapses and move along axonal microtubules, neurofilaments, and actin tracks (Kamal et al., 2001; Cirrito et al., 2008; Tampellini et al., 2009; Das et al., 2013).

MAM function has been shown to be significantly increased in fibroblasts from AD patients (Area-Gomez et al., 2012). Smaller MAMs (<10 nm) are found in hippocampal neurons in APP transgenic rats (Martino Adami et al., 2019). APP, BACE1, and γ-secretase components are all found in MAMs (Schon and Area-Gomez, 2013; Erpapazoglou et al., 2017), and MAMs bear remarkable similarity to lipid rafts, preferred subcellular microdomains for β-secretase cleavage of APP and Aβ generation (Urano et al., 2005; Vetrivel et al., 2005, 2009; Kosicek et al., 2010). Other proteins enriched in MAMs (e.g., inositol-1,4,5-trisphosphate receptor subunit 3 [IP3R3], sigma-1 receptor [S1R], and acyl-coenzyme A:cholesterol acyltransferase [ACAT]) (Schon and Area-Gomez, 2013) have emerged as AD drug targets (Bhattacharyya and Kovacs, 2010).

We recently reported APP is palmitoylated in the ER prior to localizing to lipid rafts, where it serves as a preferential substrate for cleavage by β-secretase (Bhattacharyya et al., 2013). Reduced palmitoylation leads to ER-retention and slower maturation of APP (Bhattacharyya et al., 2013). We previously showed that cortical extracts from mice exhibit age-dependent increases in palmitoylated APP (*pal*APP). Treatment with palmitoylation inhibitors (e.g., cerulenin [Cer] and 2-bromopalmitate [2-BP]) prevents APP palmitoylation and lowers Aβ production. Recently, we reported *pal*APP forms strong *cis*-dimers that undergo β-secretase cleavage in detergent resistant membranes (DRMs) or lipid rafts (Bhattacharyya et al., 2016). Loss of the ER/MAM-resident enzyme, acyl-coenzyme A:ACAT (Rusiñol et al., 1994; Lewin et al., 2002), reduces secreted Aβ by up to 92% (Puglielli et al., 2001; Hutter-Paier et al., 2004; Huttunen et al., 2007, 2010; Bhattacharyya and Kovacs, 2010; Bryleva et al., 2010; Murphy et al., 2013; Shibuya et al., 2015). ACAT inhibition decreases levels of lipid raft *pal*APP and Aβ generation by up to 76% (Bhattacharyya et al., 2013). Thus, palmitoylation plays an important role in APP metabolism and Aβ generation (Bhattacharyya et al., 2013).

Here, we investigated the role of MAMs in APP processing and trafficking and axonal generation of Aβ. We employed differentiated neurons from human neuronal progenitor cells expressing APP with familial AD (FAD) mutations (FAD hNPCs) in a three-dimensional (3D) neural cell culture model of AD (Choi et al., 2014). We also employed a biochemical assay to separate *pal*APP from non-*pal*APP and total APP ($APP_{tot}$) and developed a microfluidic system to study MAMs in axonal versus somal microenvironments in neurons. First, we show that association of *pal*APP with MAMs regulates the processing and cell surface localization of *pal*APP and Aβ generation. Second, we show that modulating MAM levels directly influences β-secretase cleavage of *pal*APP and Aβ generation. Third, we show that MAM-based generation of Aβ occurs specifically in neuronal processes and axons. These findings carry major implications for developing AD therapies based on targeting MAM-associated *pal*APP in axons to alleviate Aβ pathology.

## RESULTS

### palAPP is predominantly localized to MAMs in human neuronal cells and in mouse brains

To quantify the distribution of *pal*APP in lipid rafts versus MAMs in AD neuronal cells, we compared *pal*APP levels in flotillin-positive raft fractions (lipid rafts) versus inositol-1,4,5-trisphosphate receptor subunit 3 (IP3R3)-positive raft fractions (MAMs) in ReN-VM neural progenitor stem cells (hNPCs) constitutively overexpressing human APP containing K670N/M671L (Swedish) and V717I (London) FAD mutations ($APP_{Swed/Lon}$) (Choi et al., 2014). FAD-APP ($APP_{Swe/lon}$) expressing hNPCs (FAD hNPCs) were generated by transfecting hNPCs with IRES-mediated polycistronic lentiviral vectors encoding human $APP_{Swe/lon}$ with GFP as a reporter. Fluorescence-activated cell sorting (FACS) was employed to enrich the population. FAD hNPCs differentiated in a 3D matrix recapitulate β-amyloid and Tau pathology (D'Avanzo et al., 2015; Kim et al., 2015; Kwak et al., 2020). We metabolically labeled FAD hNPCs with chemically reactive alkylene-palmitic acid (Alkyl-C16) for 18 h, as described previously (Bhattacharyya et al., 2013). Labeled cells were subjected to sucrose gradient centrifugation (Figure 1A), and fractions were probed with the raft marker, flotillin, and MAM-marker, IP3R3. Most flotillin distributed to fraction 3, whereas most IP3R3 partitioned to fraction 4 with some overlap, indicating separation of post-ER rafts and MAMs. Although we detected equal amounts of $APP_{tot}$ in raft fractions positive for flotillin (PM-rafts) or IP3R3 (MAMs), most $APP_{tot}$ partitioned to the non-raft fractions (fractions 9 and 10) (Figure 1A), as expected. ABE palmitoylation assay revealed that ~10% of $APP_{tot}$ is palmitoylated (*pal*APP) in FAD hNPCs (Figure S1), consistent with our previous findings (Bhattacharyya et al., 2013, 2016). To detect *pal*APP distribution in FAD hNPCs, we subjected each fraction to click-iT addition of TAMRA (tetramethylrhodamine) label, as previously described (Bhattacharyya et al., 2013) (Figure 1A, click-iT palmitoylation). In flotillin-positive lipid rafts, *pal*APP constituted only 20.7% ± 3.1% of $APP_{tot}$, whereas in IP3R3-positive MAMs, *pal*APP was enriched to 68.12% ± 8.8% of $APP_{tot}$ (Figure 1B). Meanwhile, <2% of $APP_{tot}$ was palmitoylated in non-rafts fractions 9 and 10 (Figure 1B).

To confirm the localization of *pal*APP in MAMs, we extracted crude ER-mitochondria (ER-mito) from FAD hNPCs and used sucrose density gradient centrifugation to isolate MAMs (IP3R3 and ACAT-rich fractions) and non-MAMs (fractions 8–10; Figure 1C). $APP_{tot}$ distributed into both MAM and non-MAM fractions (Figure 1C). To assess *pal*APP distribution, the pooled MAM and non-MAM fractions were subjected to the recently developed Badrilla palmitoylation assay (Figure 1D). This assay captures palmitoylated proteins by exchanging palmitic acid with a thiol-bound CAPTUREome resin following thioester cleavage and isolates non-palmitoylated proteins in the CAPTUREome-unbound fractions (Figure S2). We observed strong staining for *pal*APP in MAM fractions, with little or no evidence of non-palmitoylated APP (non-*pal*APP) (Figure 1D). Conversely, non-*pal*APP was mainly distributed in the non-MAM fractions (Figure 1D). Quantitative analysis revealed ~9.8-fold more *pal*APP was associated with MAMs as compared to non-*pal*APP. In contrast, ~10.5-fold more non-*pal*APP distributed in non-MAMs compared to *pal*APP (Figure 1E). Thus, MAMs almost exclusively contain *pal*APP.

We next asked whether *pal*APP localizes to MAMs in mouse brain. Mouse brain homogenates were subjected to Percolgradient centrifugation as previously described (Wieckowski et al., 2009). Total membrane (TM), crude mixture of ER-mitochondria (ER/mito), ER, mitochondria (mito), and MAMs were isolated (Figure 1F). Equal amounts of proteins were subjected to the acyl-biotin exchange (ABE) palmitoylation assay and probed with an anti-APP antibody (C66) to detect *pal*APP in the indicated membranes (Figure 2, ABE, IB:C66). In addition to detecting APP, BACE1, IP3R3, and ACAT1 in MAMs, as previously described (Area-Gomez et al., 2009, 2012), we detected *pal*APP in MAMs (Figure 2). Thus, *pal*APP mainly resides in MAMs.

## Silencing of MAM-resident sigma 1 receptor (S1R) reduces MAM levels in FAD NPCs

S1R is a chaperone protein residing in MAMs, where it interacts with proteins such as IP3R3, which anchors the outer mitochondrial membrane protein voltage-dependent anion channel isoform 1 (VDAC1) to the ER-associated molecular chaperone glucose-regulated protein 74 (GRP74) (Hayashi and Su, 2007). Loss or inhibition of MAM-resident S1R disrupts MAM-assembly by destabilizing the MAM-resident IP3R3 (Hayashi and Su, 2007). Genetic ablation of the S1R gene in mouse brain (s*igmar1*$^{-/-}$) results in a robust decrease in IP3R3 levels and significant reduction of ER-mito contact sites (~30% of mitochondria forming MAMs in wild-type neuron versus ~18% in *sigmar1*$^{-/-}$ neurons) compared to non-transgenic control mice (Bernard-Marissal et al., 2015).

To study the effect of disrupted MAMs on the processing and β-secretase cleavage of *pal*APP, we silenced the expression of S1R in FAD hNPCs, using a SMART pool small interfering RNA (siRNA) against *sigmar1* (si-S1R) (Amer et al., 2013). We performed the CytoTox-ONE assay to measure lactate dehydrogenase (LDH) levels in the culture media to assess cell viability after introducing si-S1R for 0, 48, and 72 h. We observed ~77% reduction of S1R expression after 48 h, and >90% reduction after 72 h transfection with si-S1R. The LDH-assay revealed that 72 h transfection with si-S1R led to ~53% loss of cell viability, whereas 48 h transfection exhibited little or no reduction in cell viability (Figure S2). Cells transfected with si-S1R for 48 h were fixed and subjected to confocal and EM analyses and immune-labeling with anti-S1R antibody. Confocal microscopy revealed significant reduction of S1R expression in S1R-silenced (si-S1R) cells, compared to control cells (si-non) (Figure 2A). Equal amounts of proteins from si-non and si-S1R cells were probed for IP3R3 and ACAT1. si-S1R cells exhibited dramatic reductions of IP3R3 and ACAT1 levels compared to si-non cells (Figure 2B), indicating that silencing of S1R reduced MAM levels in FAD hNPCs. Meanwhile, S1R-knockdown had little or no effect on VDAC1, a primarily mitochondrial protein, or GRP74, a primarily ER-protein (Figure 2B), suggesting that S1R-silencing specifically affected MAMs, not bulk mitochondria or ER. Quantitation revealed ~85% reduction of S1R expression in si-S1R cells compared to si-non cells, whereas IP3R3 levels decreased by ~67% in the same cells (Figure 2C). Thus, silencing S1R expression effectively downregulates MAMs.

Next, S1R-silenced and control cells were subjected to transmission electron microscopy (TEM) to identify ER-mito contact sites or MAMs. TEM revealed robust reduction of ER-mito contact sites in si-S1R cells compared to si-non cells (Figure 2D). MAMs were

quantified directly by counting the number of ER-mito contact sites (5–20 nm size) per mitochondria per field of the electron micrographs (Bernard-Marissal et al., 2015). Quantitation revealed ~67% reduction in ER-mito contact sites or MAMs per mitochondria (MAMs per mito) in si-S1R cells versus si-non cells (Figure 2E). Thus, silencing S1R expression in FAD hNPCs significantly reduces MAM levels.

### S1R-agonist PRE-084 and S1R-antagonist NE-100 regulate MAM levels in FAD hNPCs

S1R function can be regulated using the S1R agonist PRE-084 (PRE) and antagonist NE-100 (NE) (Bernard-Marissal et al., 2015). Total IP3R3 levels were increased in the presence of 5.0 or 10.0 μM PRE and decreased following treatment with 5.0 or 10.0 μM in FAD hNPCs (Figure 2F). 10 μM PRE increased total IP3R3 levels by ~43% (1.43- ± 0.2-fold; $p < 0.05$, $n = 3$), whereas treatment with 10 μM NE decreased total-IP3R3 levels by ~20% (0.79- ± 0.08-fold; $p < 0.05$, $n = 3$) versus vehicle control (veh) cells (Figure 2G).

To confirm regulation of S1R-activity modulated MAM-associated IP3R3 levels, we isolated MAM, ER, mixed ER/mitochondria, and mitochondria fractions from FAD hNPCs following pre-treatment with 10 μM PRE or NE. The fractions were probed with antibodies against IP3R3 and cytochrome C (cyto C) to determine the purity of MAMs and of mitochondria (mito), respectively (Figure 2H). MAM-IP3R3 levels were increased (3.73- ± 0.43- fold) following treatment with PRE and significantly reduced (~55%; 0.45- ± 0.13-fold) following treatment with NE compared to veh cells (Figures 2H and 2I). The significant effects of S1R-activation or -inactivation on MAM-IP3R3 levels as opposed to the more modest effects on total-IP3R3 suggest S1R preferentially modulates MAMs in FAD hNPCs.

### Modulation of MAMs via S1R stabilizes palAPP in FAD-NPC neurons

Palmitoylation localizes and stabilizes transmembrane proteins in lipid-rich membrane compartments (Linder and Deschenes, 2007). We previously reported palmitoylation extends the half-life of APP, from $t_{1/2} = 2$ h for total APP to $t_{1/2} > 4$ h for *pal*APP, indicating *pal*APP is twice as stable as total APP (Bhattacharyya et al., 2016). To test whether association with MAMs stabilizes *pal*APP, we measured the half-life of *pal*APP in differentiated FAD-NPC neurons following upregulation of MAMs with 10 μE or downregulation with 10 μM NE. MAM-dependent *pal*APP stability was assessed by cycloheximide (CHX)-chase experiments (Bhattacharyya et al., 2016). To measure *pal*APP levels, ABE palmitoylation assays were performed after 0, 1, 2, 4, and 6 h of chase with cycloheximide (Figure 3A). ~40% of *pal*APP levels remained after 4 h chase, confirming our previous studies (Figure 3B) (Bhattacharyya et al., 2016). Treatment with PRE stabilized *pal*APP: ~90% of *pal*APP remained after the 4-h chase (Figure 3B). Conversely, treatment with NE dramatically reduced *pal*APP stability: ~20% of *pal*APP remained after 4 h of chase (Figure 3B). Meanwhile, neither PRE- nor NE-treatment altered the stability of $APP_{tot}$.

Next, we compared the half-life of *pal*APP versus non-*pal*APP using the Badrilla palmitoylation assay. We observed a marked decrease in *pal*APP levels after 4 h of chase following CHX-treatment in the control (veh) experiment (Figure 3C). A similar reduction of *pal*APP levels was observed only after 6 h of chase in cells pre-treated with PRE (Figure

3C), suggesting stabilization. Conversely, *pal*APP levels were significantly decreased in NE-treated cells (Figure 3C). 41.1% ± 2.2% of *pal*APP remained after 6 h of chase in control cells. 68.9% ± 1.7% versus 17.0% ± 1.3% of *pal*APP remained after 4 h of chase in cells pre-treated with PRE or NE, respectively (Figure 3D), whereas the stability of non-*pal*APP remained unchanged by either PRE- or NE- treatment after 4 h of chase: ~40% of non-*pal*APP remained in control, PRE-, or NE-treated cells (Figure 3E). Thus, S1R-activation specifically stabilizes *pal*APP but not $APP_{tot}$ or non-*pal*APP. Conversely, S1R-inactivation specifically destabilizes *pal*APP.

## MAM assembly regulates levels of cell surface-associated palAPP but not total APP

We next asked whether modulation of MAM assembly affects levels of cell surface-associated *pal*APP. We used a two-step pull-down assay to simultaneously detect cell surface palmitoylated and non-palmitoylated APP in FAD hNPCs, which were first surface biotinylated with sulfo-NHS-SS-biotin. Surface biotinylated-palmitoylated proteins were isolated from Neutravidin beads using *tris*(2-carboxyethyl)phosphine (TCEP) prior to carrying out the Badrilla palmitoylation assay (Figure S4). To test the effect of MAM formation on cell surface-associated *pal*APP, we performed the two-step pull-down assay in untreated FAD hNPCs and those treated with 10 μM PRE or NE (Figure 4A). We detected a robust (~1.5-fold) increase of surface labeled *pal*APP on PRE-treatment, whereas NE-treatment resulted in ~30% loss of cell surface *pal*APP (Figure 4B). In contrast, treatment with neither PRE nor NE affected cell surface biotinylation of $APP_{tot}$ or non-*pal*APP (Figures 4A and 4B). Cell surface association of the control protein transferrin receptor (Tfr) also remained unaffected following PRE- or NE-treatment (Figures 4A and 4B), consistent with Tfr being nearly absent in MAMs (Sala-Vila et al., 2016). Thus, MAM-assembly specifically promotes cell surface association of *pal*APP without affecting cell surface association of $APP_{tot}$.

## Regulation of MAM-assembly in FAD hNPCs via S1R modulates β-secretase cleavage of palAPP

Next, we asked whether silencing the expression of S1R in FAD hNPCs attenuates cleavage of APP by β-secretase. si-S1R decreased ER-mito contact sites by ~70% (Figure 2). The ABE palmitoylation assay revealed that silencing S1R significantly reduced *pal*APP levels in FAD hNPC cell lysates (Figure 5A, ABE assay, *pal*APP). In contrast, si-S1R led to no significant differences in levels of palmitoylated flotillin versus control cells (not shown) and only a small reduction in levels of $APP_{tot}$ (Figure 5A, ABE assay, $APP_{tot}$). Quantification of the reduction of *pal*APP in si-S1R cells in comparison to $APP_{tot}$ (*pal*APP/$APP_{tot}$) revealed 48.61% ± 14.60% ($p < 0.01$, $n = 3$) *pal*APP/$APP_{tot}$ in si-S1R cells as compared to si-non (Figure 5B), indicating an ~51% reduction of *pal*APP levels following S1R-silencing. We detected a smaller (14.72% ± 4.77%; $p < 0.03$, $n = 3$) decrease in $APP_{tot}$ in si-S1R cells versus si-non (data not shown), in agreement with 10%–20% of $APP_{tot}$ consisting of *pal*APP.

We next asked whether decreased *pal*APP levels following S1R-silencing affects β-secretase cleavage of APP. Conditioned media from si-non and si-S1R cells probed revealed a robust reduction in sAPPβ release relative to total sAPP following si-S1R (Figure 5A, CM, sAPPβ,

or $sAPP_{tot}$, respectively). The ratio of sAPPβ/$sAPP_{tot}$ in conditioned media from si-S1R cells was 44.62% ± 16.84% ($p < 0.01$, n = 3) of that observed in si-non cells (Figure 5B), with an ~58% reduction in sAPPβ release following si-S1R. Thus, ~70% downregulation of MAM-assembly following silencing of S1R leads to significant reduction in β-secretase cleavage of APP, most likely by reducing *pal*APP levels.

Next, we measured *pal*-sAPPβ release from FAD hNPCs treated with 10 μM PRE or NE. Figure 4D shows that treatment with PRE increased MAM-IP3R3 levels by ~3.7-fold, whereas NE decreased MAM-IP3R3 levels by ~45%. Next, *pal*-sAPPβ levels were assessed by the ABE palmitoylation assay as done before (Bhattacharyya et al., 2013). Treatment with PRE led to a significant increase in *pal*-sAPPβ release compared to veh cells (Figure 7C, ABE, IB:anti-sAPPβ). In contrast, *pal*-sAPPβ release was dramatically decreased following treatment with NE (Figure 5C, ABE, IB:anti-sAPPβ). Neither PRE nor NE-treatment led to any significant effect on total sAPP ($sAPP_{tot}$) or sAPPβ release (Figure 5C), nor on APP-C-terminal fragment (CTF) levels (Figure S6). In comparison to $sAPP\beta_{tot}$-release, *pal*-sAPPβ (*pal*-sAPPβ/$sAPP\beta_{tot}$) was increased by 2.14- ± 0.39-fold ($p < 0.001$, n = 3) following treatment with PRE (Figure 5D). Conversely, NE-treatment reduced *pal*-sAPPβ release by ~50% (0.508- ± 0.073-fold as compared to control, $p < 0.001$, n = 3) (Figure 5D). Thus, modulation of MAM levels via S1R specifically affects β-secretase but not α-secretase cleavage of *pal*APP and does not affect β- and α-secretase cleavage of $APP_{tot}$.

## Regulation of S1R-activity specifically modulates MAMs in neuronal processes

To test for S1R-dependent changes in MAM-assembly in neuronal processes versus cell bodies, we performed confocal microscopy to visualize the ER-mito contact sites in cells pre-labeled with cell-permeable GFP-tagged ER (CellLight ER-GFP) and RFP-tagged mitochondrial (CellLight mito-RFP) probes. A MAM-resident $Ca^{2+}$-sensor protein Miro has been shown to be co-transported with mitochondria down axons (Misko et al., 2010). Elevated calcium levels halt axonal transport of Miro, indicating MAM-transport along axons could be regulated by physiological stimuli (Macaskill et al., 2009; Wang and Schwarz, 2009).

We first confirmed that the GFP- and RFP-tagged probes could correctly identify ER-mito contact sites in mouse cortical neurons from C57BL/6 embryonic day 16 (E-16) mice. Confocal microscopy revealed that ER-GFP (green fluorescence) and mito-RFP (red fluorescence) distinctly labeled ER and mitochondria, respectively, in cell bodies as well as in processes (Figure 6A, a–c). The overlapping areas between ER and mitochondria (ER-mito) were identified as MAMs (Figure 6A, d, white arrow). Employing a modified MAM-imaging technique (Filadi et al., 2015) that eliminated all non-overlapping fluorescence (representing ER and mitochondria), we were able to highlight the contact areas (white) (Figure 6A, e–g) and demonstrated MAMs in the processes (Figure 6A, h–j) as well as in cell bodies (Figure 6A, k–m).

ER-mito contact sites >10 nm in both processes (Figure 6A, n–p) and in cell bodies (not shown) were counted as MAMs, using the ImageJ particle measurement tool. Quantitation of MAMs (ER-mito contact sites) revealed that treatment with 10 μM PRE increased MAMs in axons and neuronal processes by ~2.5-fold, without affecting MAMs in the cell bodies or

soma of cultured primary neurons (Figure 6B). Conversely, treatment with 10 μM NE decreased ER-mito contact sites by ~50%, only in axons and neuronal processes (Figure 6B). Similar results were obtained when we counted ER-mito contact sites in neuronal processes of FAD hNPCs pre-labeled with the ER and mitochondria probes (Figure 6C). NE-treatment decreased ER-mito contact sites, whereas treatment with PRE increased ER-mito contact sites, primarily in neuronal processes, without altering ER-mito contact sites in cell bodies (Figure 6D). We next used a bidirectional fluorescent compensation (BiFC) assay to assess the effect of S1R-inactivation on axonal MAMs in cells co-expressing split GFP ER and mitochondria probes (ER-GFP(1–10) and mito-GFP11, respectively) (Yang et al., 2018). NE treatment reduced the number of MAMs per axon by ~35% (from 27.87 ± 1.52 MAMs/axon in control to 3.125 ± 1.23 MAMs/axons in NE-treated) (Figure S6). Thus, modulation of S1R activity regulates MAM assembly specifically in axons and neuronal processes, not in the cell body or soma.

To further validate that pharmacological regulation of S1R specifically affects axonal MAMs, we developed a microfluidic device (Figure 6E) that separates bulk neurons from axons following physical axotomy (Figure 6F). Although we accumulated a sufficient number of axons from 10 devices to obtain detectable levels of MAM-resident proteins including IP3R3, ACAT, and VDAC1 (Hedskog et al., 2013; Liu et al., 2019), this number of axons was insufficient for MAM purification. Thus, we assessed MAM levels in axons by measuring total levels of MAM-resident proteins, IP3R3, ACAT, and VDAC1, following axotomy (Figure 6G). We confirmed that the axonal fractions were not contaminated with bulk neurons following axotomy, by probing the fractions with an antibody against the nuclear envelope protein, lamin B1 (Figure 6G, IB:anti-lamin B1). We observed significant increases in all levels of all three axonal MAM-proteins measured following treatment with 10 μM PRE versus veh cells (Figure 6G). Conversely, the levels of all three MAM-proteins were dramatically reduced in axons following treatment with 10 μM NE (Figure 6G). Meanwhile, treatment with either PRE or NE had little or no effect on levels of IP3R3, ACAT, and VDAC1 in bulk neurons (Figure 6G). Quantitative analysis revealed that treatment with PRE increased levels of MAM-resident IP3R3, ACAT, and VDAC1 in the axons by 3.16- ± 0.41-fold, 1.4- ± 0.18-fold, and 1.79- ± 0.11-fold, respectively, as compared to axons from veh cells (Figure 6H). Conversely, axons from NE-treated cells contained 25% (0.25- ± 0.09-fold) IP3R3, 21% (0.21- ± 0.03-fold) ACAT, and only 3% (0.03- ± 0.008-fold) VDAC1 compared to veh cells (Figure 6H).

## Modulation of MAMs in neuronal processes/axons regulates axonal Aβ generation from FAD hNPCs

APP and amyloidogenic processing enzymes, β- and γ-secretases, are localized in axons and dendrites (Kaether et al., 2000), and anterograde axonal transport delivers Aβ and sAPPβ to neurites around amyloid plaques. Axons have been heavily implicated in AD-related Aβ-generation and tau phosphorylation (Kamal et al., 2001; Cirrito et al., 2008; Tampellini et al., 2009; Das et al., 2013). Thus, we next investigated whether MAM-assembly in neuronal processes and axons affects Aβ generation. To measure axonal Aβ release, we employed a microfluidic chamber system (Xona Microfluidics) to perform fluidic separation of cell somas from axons in differentiated FAD hNPCs (Niederst et al., 2015). In this system,

capillary channels draw axons from the somal chamber into the axonal chamber. To prevent cells from migrating into the axonal chamber, we plated FAD hNPCs in a 3D matrix on the somal side prior to differentiation. Both somal and axonal chambers were probed either with Hoechst dye to label the nuclei or with antibody against tau and/or neurofilament heavy (NFH) antibodies to label axons (Figure 7A, tau and NFH). We then carried out microfluidic isolation of the axonal microenvironments from bulk neuronal environments by establishing a small (30 μL) volume difference between axonal and somal compartments (Taylor et al., 2005). After 10–15 days in differentiating media, conditioned media from each chamber was subjected to Aβ ELISA to detect $A\beta_{40}$ levels ($A\beta_{42}$ levels were below detection limit). Levels of $A\beta_{40}$ in the somal chamber reached 372.4 ± 50.7 pM per chamber in 24 h. To account for axonal $A\beta_{40}$ in the somal chambers, we determined axonal numbers by subtracting the number of tau-positive axons in the axonal chambers from the number of cells (~30,000 DAPI-stained nuclei in the somal chambers) in the somal chambers, assuming each cell produced only one axon. $A\beta_{40}$-release in the axonal chambers was then calculated as the number of $A\beta_{40}$ molecules per tau-positive axon, using a previously described method of measurement (Niederst et al., 2015). We found differentiated FAD hNPC neurons generated $10.69 \times 10^8 \pm 4.2 \times 10^8$ $A\beta_{40}$ per cell bodies and $2.97 \times 10^8 \pm 5.3 \times 10^6$ $A\beta_{40}$ per axon in 24 h (Figure 7B).

Next, we pharmacologically modulated MAM assembly and tested for effects on Aβ generation in neuronal processes/axons versus neuronal cell somas. We measured $A\beta_{40}$ levels in the somal and axonal chambers of 10- to 15-day differentiated FAD hNPCs in microfluidic systems that received either vehicle (veh), 10 μM PRE, or 10 μM NE for 24 h. Neither PRE- nor NE-treatment altered $A\beta_{40}$ levels in the somal chamber. However, PRE treatment increased the number of $A\beta_{40}$ molecules released per axon by an additional $11.63 \times 10^8 \pm 9.2 \times 10^7$. In contrast, NE treatment reduced axonal $A\beta_{40}$ release to nearly undetectable levels (Figure 7B). Thus, modulation of MAM levels governs Aβ generation, specifically in axons and neuronal processes, but not in the cell soma.

## DISCUSSION

We have previously shown that palmitoylation of APP targets *pal*APP to lipid rafts where it becomes a preferred substrate for β-secretase. Here, we show that *pal*APP is primarily localized to specialized lipid rafts known as MAMs, in both FAD hNPCs and in mouse brain. We also show that genetically silencing or pharmacologically inactivating the MAM-resident receptor, S1R (with the S1R-antagonist NE100) to downregulate MAM assembly (by destabilizing MAM-resident IP3R3), leads to greatly decreased levels of *pal*APP, reduced stability and cell surface trafficking of *pal*APP, decreased β-secretase cleavage of *pal*APP, and reduced generation of sAPPβ and Aβ. In contrast, the S1R-agonist PRE-084 upregulated MAM levels and increased *pal*APP stability and cell surface trafficking, β-secretase cleavage of *pal*APP, and Aβ generation. Furthermore, we show that modulation of S1R regulates MAM assembly, stability, and cell surface trafficking of *pal*APP, β-secretase cleavage of *pal*APP, and Aβ generation specifically in axons. Thus, we demonstrate a clear connection between MAM-assembly and Aβ generation from *pal*APP, specifically in axons and neuronal processes.

Previous studies have shown that SigR1 knock out (*Sigmar1*$^{-/-}$) decreases MAM-assemblies by nearly 50% (Bernard-Marissal et al., 2015). We demonstrated that silencing of S1R expression not only reduces MAMs (Figure 2) but also reduces the levels of *pal*APP with minimal to no effects on $APP_{tot}$ levels (Figure 5A). We have previously shown that *pal*APP and/ or *pal*APP-dimers are better substrates for β-secretase cleavage in lipid-rich microdomains as compared to $APP_{tot}$ (Bhattacharyya et al., 2013, 2016). Here, we show that levels of sAPPβ were reduced with silencing of MAM-resident S1R expression, and regulation of S1R activity by an agonist (PRE-084) or an antagonist (NE-100) not only modulates MAMs (Figure 2), but also specifically promotes or reduces β-secretase cleavage of *pal*APP, respectively (Figures 5C and 5D). Thus, MAMs and palmitoylation of APP directly modulate β-secretase cleavage of *pal*APP and subsequent Aβ generation.

The observation that S1R activation and inactivation oppositely modulate the stability of *pal*APP with no effects on $APP_{tot}$ (Figure 3) is consistent with previous studies reporting evidence for palmitoylation-dependent stability of transmembrane proteins in lipid-rich membranes (Linder and Deschenes, 2007). Here, we show that modulation of S1R-activity affects cell-surface association of *pal*APP without affecting that of $APP_{tot}$ (Figure 4). Although it remains unclear how association with MAMs promotes the cell surface association of *pal*APP, it is worth noting that ~11% of MAM-proteins are found in the plasma membrane (Poston et al., 2013). Additionally, MAM-like ER-rafts fusing with plasma membrane, called PAMs, have been detected in several tissues involved in regulating $Ca^{2+}$ homeostasis, lipid trafficking, and mitochondrial structures (Szymański et al., 2017).

We also showed S1R activity mainly modulates MAM levels in axons and neuronal processes as opposed to neuronal cell bodies and soma (Figure 6). Thus, S1R-activity specifically regulates the assembly of a novel subset of MAMs enriched in axons and neuronal processes, while the assembly of MAMs in cell bodies is independent of S1R-activity. A previous study reported that S1R knockout only reduced MAM-assemblies in neurons by >50%, suggesting that more than half of MAM-assemblies were independent of S1R activity (Bernard-Marissal et al., 2015). Moreover, MAMs also differ in size and motility (Volpe et al., 1991; Bannai et al., 2004). We discovered that modulation of MAMs in neuronal processes via alteration of S1R-activity specifically affects β-secretase cleavage of *pal*APP without affecting cleavage of total $APP_{tot}$ (Figures 5 and S5). Small molecule agonists and antagonists of S1R are currently being considered as therapeutics for numerous neurodegenerative diseases (Ryskamp et al., 2019).

Using a system incorporating FAD gene-expressing hNPCs grown in a 3D matrix inside microfluidic chambers, we were able to reveal that S1R regulates MAM-dependent Aβ generation exclusively in axons and neuronal processes, but not in soma or from bulk neurons (Figure 7). Axons and synapses are critical sites for APP-processing and Aβ production. (Lazarov et al., 2002; Sheng et al., 2002; Brendza et al., 2003; Spires et al., 2005). Previous studies have shown that intra-axonal Aβ is generated ahead of extracellular Aβ especially when axons are under stress (Suo et al., 2004). Moreover, amyloid deposition has been reported to decrease when β-secretase processing of APP and Aβ generation is shifted away from axonal to somal compartments (Lee et al., 2005). A recent study reported that ER-mitochondria tethering is increased in axons following injury (Lee et al., 2019).

Here, we show that axons specifically use MAMs, containing ~70% of preferred β-secretase substrate, *pal*APP, to generate Aβ. Other studies have reported that Aβ and/or the β-cleaved C-terminal fragment of APP (C99 or APP-βCTF) modulate MAM function in AD (Schreiner et al., 2015; Pera et al., 2017). Knocking down the expression of MAM-resident mitofusin 2 (Mfn 2) resulted in increased ER-mito contact and decreased levels of Aβ (Leal et al., 2016). Our data reveal an additional converse mechanism whereby modulation of MAMs regulates Aβ generation in axons and neuronal processes. Collectively, these findings suggest a possible feed-forward mechanism for MAM-dependent AD pathogenesis.

The subcellular location in which APP primarily undergoes β-secretase cleavage in neurons has remained a topic of intensive investigation. We previously reported that APP undergoes palmitoylation targeting it to lipid rafts where it serves as a preferential substrate for β-secretase. In addition to lipid rafts in plasma membranes, intracellular MAMs have been increasingly investigated in neurodegenerative diseases such as AD and amyotrophic lateral sclerosis. We previously reported that reduced palmitoylation leads to ER-retention of APP. Here, we expand on these findings by showing that most *pal*APP is partitioned to MAMs. We and others have previously shown that the loss or inhibition of the MAM-resident enzyme acyl-co-enzyme A:ACAT reduces cell surface localization of APP and Aβ generation (Huttunen et al., 2009; Bhattacharyya and Kovacs, 2010; Murphy et al., 2013). More recently, we showed that inhibition of ACAT reduces *pal*APP in lipid-rafts by ~76%, *in vitro* (Bhattacharyya et al., 2013). Palmitoylation inhibitors 2-bromopalmitate and cerulenin also reduced *pal*APP level and Aβ generation *in vitro* (Bhattacharyya et al., 2013, 2016). Confocal imaging revealed that cerulenin (Cer) treatment reduced APP distribution in axonal MAMs (IP3R3-labeled), but not in somal MAMs in differentiated PC12 and NPCs (Figure S7). Based on these data, we propose that *pal*APP partitions into axonal MAMs, whereas total or de-palmitoylated APP resides in somal MAMs. Future studies will be needed to explore whether palmitoylation inhibition as well as ACAT inhibition ameliorates β-amyloid pathology by reducing *pal*APP levels specifically in axonal MAMs.

In this study, we used FAD hNPCs expressing the FAD mutant of APP ($APP_{Swe/Lon}$) to examine the role of MAM-association of *pal*APP in axonal Aβ generation. Lipid raft fractionation, cell surface biotinylation, and ABE palmitoylation assays (Figures 1A, 4A, and S1) have confirmed that the overall cellular localization and palmitoylation of total APP in FAD hNPCs remain similar to those observed *in vitro* and *in vivo* (Bhattacharyya et al., 2013, 2016). These observations suggested that the Swedish and the London mutations in APP do not affect APP's overall cellular localization or palmitoylation. Several reports have shown that Swedish and/or London mutations in APP in non-neuronal (MDCK and COS) and neuronal (SN56) cells altered the endocytosis of APP without altering its cell surface association. The $APP_{swe}$ mutant has been shown to undergo β-secretase cleavage in secretory vesicles en route to the cell surface, whereas $APP_{wt}$ undergoes β-secretase cleavage in post-Golgi compartments after endocytosis (Haass et al., 1995). The Swedish and London mutations in APP slowed the rapid transport from cell surface to lysosomes required for APP-degradation (Lorenzen et al., 2010). In a recent study using the iPSC neurons, Kwart et al. (2019) have shown that CRISPR/Cas9-edited cells expressing $APP_{Swe}$ have promoted enlargement of Rab5-positive endosomes, which is an early hallmark of AD (for review, see Peric and Annaert, 2015). Therefore, it would be interesting in future studies

to investigate whether the Swedish/London mutations in APP ($APP_{Swe/Lon}$) affect endocytosis of *pal*APP to lysosomes or alter endosome size in AD.

The degree of dementia in AD is primarily correlated with loss of synapses. Synaptic dysfunction, preceded by reduced synaptic transmission and loss of dendritic spines, is largely driven by neurotoxic $A\beta_{42}$-oligomers (Cleary et al., 2005; Haass and Selkoe, 2007). Physiological levels of $A\beta_{42}$-oligomers have also been shown to suppress long-term potentiation (LTP) in hippocampal slices (Mango et al., 2019). In contrast, Aβ in the picomolar range has also been shown to be required for LTP induction (Koppensteiner et al., 2016). Thus, a key question regarding AD pathology is how Aβ is generated in axons and neuronal processes. Previous studies have shown that APP can be transported anterogradely in axons (Koo et al., 1990; Sisodia et al., 1993; Buxbaum et al., 1998), and Aβ can be made in axonal terminals (Cirrito et al., 2005). To date, the cellular and molecular mechanisms by which this critical pool of axonal Aβ is generated have remained unclear. Our microfluidic chamber system showed that Aβ may be released from axons even in the absence of synapses. This observation is in line with several reports showing focally increased toxic Aβ species in axonal swellings of dystrophic neurons in AD (Stokin et al., 2005; Chevalier-Larsen and Holzbaur, 2006; Kanaan et al., 2013). We reason that MAM-upregulation in axons promotes focally increased secretion of Aβ species from regions along the axons. Axonal swelling along axons has been reported at the early stage of AD pathology leading to axonal dysfunction and Aβ deposits surrounding dystrophic neurons in later stage of the disease (Teipel et al., 2007; Cross et al., 2008; Serrano-Pozo et al., 2011). The mechanisms in the early phase leading to axonal damage in AD pathology remain unclear. MAM dysregulation is an early event in AD pathogenesis (for review, see Yu et al., 2021). Axonal BACE1 levels were increased in axonal swellings in an AD mouse model by genetic deletion of an adaptor protein GGA3, which regulates lysosomal degradation of BACE1, leading to increased production of Aβ (Lomoio et al., 2020). Thus, Aβ released from axons (even in the absence of synapses) is likely to impact AD pathogenesis. In summary, we have demonstrated that axonal Aβ generation is specifically modulated by MAMs via stabilization and cell surface trafficking of *pal*APP, followed by β-secretase cleavage. These data strongly suggest that modulation of MAM-associated *pal*APP, specifically in axons (e.g., by regulation of S1R), may be considered a therapeutic strategy for ameliorating Aβ-induced neurodegeneration in AD.

## STAR★METHODS

Detailed methods are provided in the online version of this paper and include the following:

### RESOURCE AVAILABILITY

**Lead contact—**Further information and requests for resources and reagents should be directed to and will be fulfilled by the Lead Contact, Rudolph E. Tanzi (email: tanzi@helix.mgh.harvard.edu).

**Materials availability—**All expression vectors used in this study are available upon request.

**Data and code availability—**All data are available in the manuscript or in the supplementary materials.

## EXPERIMENTAL MODEL AND SUBJECT DETAILS

We have used ReN-VM neural progenitor stem cells (hNPCs) constitutively overexpressing human APP containing K670N/M671L (Swedish) and V717I (London) FAD mutations ($APP_{Swed/Lon}$) (Choi et al., 2014). FAD-APP ($APP_{Swe/lon}$) expressing hNPCs (FAD hNPCs) were generated by transfecting naive hNPCs with IRES-mediated polycistronic lentiviral vectors encoding human $APP_{Swe/lon}$ with GFP as a reporter for viral infection. Fluorescence-activated cell sorting (FACS) was employed to enrich the population. FAD hNPCs differentiated in 3D matrix were thoroughly characterized as one of the most effective cellular models tha mimicked amyloid pathology of human AD (D'Avanzo et al., 2015; Kim et al., 2015; Kwak et al., 2020). In addition, mouse cortical neurons from C57BL/6 embryonic day 16 (E-16) mice (female) were used to confirm effect of S1R-modulation on axonal and somal MAMs. All experiments involving animals were performed accordance to the guidelines for animal welfare approved by Institutional Animal Care and Use Committee (IACUC) of Harvard University.

## METHOD DETAILS

**Isolation of lipid rafts—**For lipid raft fractionation from FAD hNPCs, cells were plated on thin-layer 3D matrix (1:10 Matrigel containing culture media), routinely used as a cellular model for AD (Kim et al., 2015). Lipid rafts were isolated from 0.5% Lubrol WX lysates of 10-day differentiated FAD hNPCs following published protocol (Bhattacharyya et al., 2013). To isolate ER-lipid rafts or MAMs, we first prepared crude Mitochondria fractions (Annunziata et al., 2013, 2018) prior to sucrose gradient centrifugation to isolate MAMs and non-MAMs. Briefly, 90% confluent cultured differentiated neuronal cells were resuspended in 5-volume homogenization buffer (10mM HEPES, pH 7.4, 0.25 M sucrose, protease inhibitors). The suspension was homogenized by 20-strokes in a glass homogenizer twice. Removing cell debris and nuclei after centrifugation (600 X g for 5min), the supernatant was subjected to sequential centrifugation steps as described before (Wieckowski et al., 2009) to isolate crude mitochondria (containing ER-rafts or MAMs) by discarding plasma membrane, lysosomes, microsomes and the cytosol. The crude mitochondria pellet was suspended in 0.5% Lubrol in 50 mM HEPES pH 7.4 containing 0.15 M NaCl, 5mM EDTA and protease inhibitor prior to sucrose gradient centrifugation as described before (Bhattacharyya et al., 2013). 1ml fractions were gently collected from the top of the gradient before immunoblotting with antibodies against MAM-proteins IP3R3 (anti-IP3R3) or ACAT (anti-ACAT) to determine MAM and non-MAM fractions.

**Isolation of MAMs (mitochondria-associated ER membrane)—**Purification of ER, mitochondria and MAMs from cultured cells were performed and analyzed as described (Area-Gomez et al., 2009). Briefly, FAD hNPCs were plated over a thin-layer 3-D matrigel matrix as described before (D'Avanzo et al., 2015), prior to differentiation. 10-day differentiated FAD hNPCs were harvested in resuspension buffer (5 mM HEPES, pH 7.4, 250 mM Manitol and 0.5 mM EGTA). Crude ER membranes were isolated after sequential centrifugation. Crude mitochondria containing MAM and Mito were layered on 30% Percol

gradient prior to centrifugation at 100,000 g for 30 min. The upper layer containing MAMs were diluted and further centrifuged at 100,000 g for 1 hr to isolate pure MAMs. Purity of MAMs in the MAM-fractions was measured by immunoblotting the fractions with antibody against MAM-resident IP3R3 antibody (anti-IP3R3) as was done before (Area-Gomez et al., 2009). Probing the fractions with antibody against the mitochondrial marker cytochrome C (anti-Cyto C) showed little or no distribution of cytochrome C (Cyto C) in the MAM fractions, confirming purity of the isolated MAMs. Anti-Cyto C, however, detected Cyto C in both crude ER and mitochondria fractions.

We isolated MAMs from mouse brains following published methods (Wieckowski et al., 2009). We collected brains from non-transgenic (non-Tg) mice (C57BL/6J background). All animal handling and tissue harvesting were performed in accordance with the guidelines of Massachusetts General Hospital Animal Care Use Committee. Mice used in this study were of either sex. Three-month old mice were sacrificed, and brains were immediately removed and stored at −80°C. Briefly, mouse brains were homogenized in five volumes of homogenization buffer prior to fractionation and Percol density gradient centrifugation to isolate pure MAMs. Isolation of pure MAMs were confirmed by determining the presence of MAM-proteins such as IP3R3 and ACAT1, and absence of mitochondrial Cyto C.

**Metabolic labeling with Alkyl-C16—**Briefly, cells were metabolically labeled with a chemical palmitic acid probe, alkylene palmitic acid (Alkyl-C16; Invitrogen) as described previously (Bhattacharyya et al., 2013). Six hours after labeling, cells were subjected to sucrose-density gradient centrifugation to collect lipid rafts and non-rafts. APP was pulled-down from the fractions using anti-APP C-terminal antibody (C66) prior to addition of a biorthogonal alkyne-labeled fluorescent chromophore, tetramethylrhodamine (alkyne-TAMRA; Invitrogen) via “click chemistry.” The samples were then probed with an anti-TAMRA antibody (Invitrogen).

**ABE palmitoylation assay—**This assay is based on previously described three-step chemical method where free unmodified cysteine thiols are blocked with NEM (N-ethyl maleimide) followed by palmitoylation thioesters cleavage by hydroxylamine ($NH_2OH$); finally, loading thiol-specific biotinylating reagent (HPDP-biotin in our experiments) to the newly exposed cysteinyl thiols. Biotinylated proteins are then affinity purified with streptavidin–agarose beads and probed for the protein of interest (Bhattacharyya et al., 2013). The assay was performed on total cell lysates extracted from differentiated FAD NPCs. In some cases, cells were treated with sigma1 receptor (S1R) agonist PRE-084 or antagonist NE-100 before ABE assay. ABE assays were also performed on cells undergoing cycloheximide (CHX) chase for 0–18h. For lipid raft, MAMs and non-raft palmitoylation studies, protein extracts from lipid rafts, MAMs and non-rafts were subjected to ABE assay according to a method reported previously (Bhattacharyya et al., 2013). Briefly, lipid raft and MAM fractions were extracted with 60 mM n-Octylglucoside (Sigma), and non-raft fractions were extracted with 1% Triton X-100. The protein extracts were precipitated using chloroform/methanol before ABE assay.

**Badrilla palmitoylation assay—**Palmitoylation assay was performed using CAPTUREome S-Palmitoylated Protein assay kit from Badrilla, UK, following the

manufacturer's protocol. This assay used the technique employed in ABE assay with some exceptions. It replaced the biotinylating step of ABE assay with direct conjugation of thioester-cleaved palmitoylated proteins with CAPTUREome resin containing thiol-reactive groups. This resulted in the covalent capture of proteins on a resin, permitting more stringent treatment to harvest S-acylated proteins with ease and high purity. Most importantly, due to the absence of the biotinylation step in ABE assay, this assay was able to not only capture palmitoylated proteins but also was able to capture cell surface biotinylated palmitoylated proteins. In addition, we were also able to isolate non-palmitoylated proteins in the unbound fractions from CAPTUREome precipitates. Briefly, cells were lysed in presence of a blocking reagent before extraction. S-palmitate groups were removed via cleavage of thioester bonds, by incubating the cell extracts with the thioester cleavage reagent. This resulted in the creation of free thiol groups on proteins where the palmitic acid group used to be. As a control, the cell extracts were incubated with acyl prevention reagent. After incubation, CAPTUREome captures resin containing reactive thiol group was added to both control and samples containing thioester cleavage reagent. After washing three times, pulled-down samples were immunoblotted with appropriate antibodies to test palmitoylation. Proteins captured by CATUREome from samples treated with thioester reagent represented palmitoylated proteins. Unbound fractions were subjected to two sequential CAPTUREome precipitation to remove all palmitoylated protein, while the proteins in the final unbound fractions contained non-palmitoylated proteins. In some cases, the assay was performed on MAMs and non-MAMs isolated from sucrose gradient centrifugation of the ER-mitochondria extract of FAD hNPCs.

**Cell surface biotinylation assay of palmitoylated proteins—**This assay was a combination of cell surface biotinylation and Badrilla palmitoylation assays. Covalent attachment of cell surface proteins with cell impermeable thiol-cleavable amine-reactive biotinylation reagent (EZ-link sulfo-NHS-S-S-Biotin, Thermo Scientific) was a technique to monitor trafficking of proteins to the cell surface. Badrilla assay of cell surface biotinylated proteins were designed to detect palmitoylated proteins at the cell surface. The combined assay was performed in two steps. First, cultured cells were subjected to cell surface biotinylation assay following published protocol (Sannerud et al., 2011). Briefly, cultured cells were placed on ice to restrict endocytosis prior to labeling with 0.5 mg/ml biotin reagent for 60 min. Cells were then washed and the unbound biotin reagent was quenched with 100 μM lysine for 5 min. After three-washes with PBS, cells were lysed with extraction buffer containing 10mM Tris (pH 7.4), 2mM EDTA, 150mM NaCl, 1% Triton X-100, 0.5% sodium deoxycholate, 0.2% SDS, and protease inhibitors. 750 μg of cell extract was subjected to pull-down with Neutravidin beads to purify biotinylated cell surface proteins. Proteins were extracted from the beads either by incubating with SDS sample buffer containing 0.1% β-mecrcaptoethanol (βME) or by extracting with 25mM TCEP solution in 50mM Tris-buffer, pH 8.5. βME-extracted samples were probed with appropriate antibodies to detect cell surface association of APP (C66 antibody), transferrin receptor (anti-Tfr antibody) or $\beta_2$ adrenergic receptor (anti-$\beta_2$AR antibody). Next, the TCEP purified cell surface proteins were subjected to Badrilla palmitoylation assay to detect palmitoylated proteins at the cell surface. CAPTUREome-bound proteins constituted palmitoylated cell surface proteins. APP and $\beta_2$AR were detected in the CAPTUREome bound fractions

showing cell surface palmitoylated APP and $\beta_2$AR at the cell surface. We used transferrin receptor as a positive control for cell surface biotinylation assay, and a negative control for cell surface Badrilla assay because Tfr was not palmitoylated. CAPTUREome beads did not pull-down Tfr confirming the efficiency of the combined assay to detect palmitoylated proteins at the cell surface. The combined assay was performed on cells untreated (veh) or pre-treated with S1R-agonist (PRE- 084) or antagonist (NE-100).

**Cycloheximide chase assay—**Cultured cells were incubated with 100 μM cycloheximide (CHX, Sigma) for various times, as described before (Dai et al., 2013). Cell lysates were prepared for ABE or Badrilla Palmitoylation assays prior to western blot analysis. In some cases, CHX-chase were performed in cells treated with 10 μM PRE or NE.

**Confocal microscopy—**Differentiated hNPCs, FAD hNPCs and primary neurons were grown on coverslips or inside microfluidic chamber slides prior to labeling with antibodies following methods described before (Bhattacharyya et al., 2016). Briefly, cells were fixed in 4% paraformaldehyde (PFA) prior to labeling with antibodies against S1R, tau or pNFH followed by appropriate fluorescence conjugated secondary antibodies. Fluorescence microscopy was performed under Nikon confocal microscope using 40X objective. Images were processed by ImageJ software.

To determine MAM-assemblies, cells were incubated with membrane-permeable ER and mitochondria probes (Cell Light ER-GFP and Cell Light Mito-RFP, respectively) for 16h prior to confocal microscopy. Cell Light reagents (Thermo Fisher) containing 1 X $10^8$ particles/ml were used. We used 25 particles per cell (PPC) of each probe. Precisely, we differentiated 40,000 cells and probed with 10 μL of Cell Light ER-GFP or Cell Light Mito-RFP. Confocal images were processed by Photoshop to eliminate GFP and RFP signals by minimizing the saturations to zero without altering the GFP and RFP overlapped regions. We highlighted the overlapped regions white that represented the ER-mitochondria contact sites or MAMs. Next, we measured the number of ER-Mito sites or MAMs using ImageJ software. Specifically, we used “analyze particle and image calculator” option to measure the number of areas > 10 nm because the sizes of MAMs ranged between 5 and 20 nm (Szymański et al., 2017). We counted the number of MAMs in cell bodies, as well as in the neuronal processes. The mean of the MAM-counts was used for quantification of MAMs in cell bodies and in neuronal processes.

**Bio-immunofluorescence (BiFC) assay—**Bio-immunofluorescence of split GFP constructs (BiFC) assay was performed as done before (Bhattacharyya et al., 2016). We have used expression plasmids encoding split-GFP (spGFP) BiFC probes for ER and mitochondria. Specifically, we transiently transfected (Lipofectamine 2000, Invitrogen) plasmids encoding spGFP(1–10)-tagged ER protein Ubc6 [ER-GFP(1–10)] and a spGFP11-tagged mitochondrial protein Tomm70 (Mito-GFP11) (Yang et al., 2018). The plasmids are generous gifts from Dr. Chao Tong, Professor, Life Sciences Institute, Zhejiang University, China. Co-expression of these probes hNPCs resulted in punctate GFP-signals confirming close contacts between these 2 organelles, suggesting detection of MAMs. Cells were then treated with S1R-antagonist NE-100 for 16 h before fixing in 4% paraformaldehyde in 1x PBS at room temperature (RT) for 30 min. Fluorescence microscopy was performed under

Nikon confocal microscope using 60X objective. The fluorescent puncta in axons and in cell bodies were counted and plotted to determine the effect of NE-100 on the number of MAMs per axon or per cell body. We assessed the expression of ER- and Mito-probes by labeling with anti-GFP antibody. BiFC puncta in the cell bodies or in axons of 20 untreated and 20 treated cells were counted for analysis.

**Transmission electron microscopy—**Transmission Electron Microscopy of cells containing control non-targeting siRNA (si-non) or siRNA against S1R (si-S1R) were performed at the Harvard Medical School Electron Microscopy Core facility. Briefly, cells were fixed in routine fixative containing 2.5% Glutaraldehyde 2.5% Paraformaldehyde in 0.1 M sodium cacodylate buffer (pH 7.4) overnight at 4°C. Cells were then washed in 0.1M Sodium cacodylate buffer pH 7.4, post fixed for 30 min in 1% Osmium tetroxide (OsO4)/ 1.5% Potassium ferrocyanide (KFeCN6), washed in water 3x and incubated in 1% aqueous uranyl acetate for 30min followed by 2 washes in water and subsequent dehydration in grades of alcohol (5min each; 50%, 70%, 95%, 2× 100%). Cells were removed from the dish in propylene oxide, pelleted at 3000 rpm for 3min and infiltrated for 2hrs to ON in a 1:1 mixture of propylene oxide and TAAB Epon (Marivac Canada Inc. St. Laurent, Canada). The samples subsequently embedded in TAAB Epon and polymerized at 60°C for 48 hr. Ultrathin sections (about 60nm) were cut on a Reichert Ultra cut-S microtome, picked up on to copper grids stained with lead citrate and examined in a JEOL 1200EX Transmission electron microscope or a TecnaiG$^2$ Spirit BioTWIN and images were recorded with an AMT 2k CCD camera. We manually counted the ER-mitochondria (ER-Mito) contact sites > 10 nm per mitochondria per frame as described before (Bernard-Marissal et al., 2015). We counted more than 25 frames. Average of the counts were used to quantitate the fold decrease of ER-Mito contact sites or MAMs in S1R-silenced (si-S1R) cells compared to control (si-non) cells.

**Microfluidic two-chamber device design and fabrication—**The microfluidic chips composed of two distinct chambers connected through microgroove arrays (5 × 8 × 450 mm in height, width and length) were fabricated using standard soft photolithography techniques (Qin et al., 2010). Briefly, the master for preparing the PDMS array was microfabricated with SU-8 photoresist (MicroChem Co.) on a silicon wafer. The first layer (5 μm depth) contained 195 microgrooves and the second layer (100 μm depth) of SU-8 contained the compartments were patterned by photolithography using high-resolution chromium masks. The PDMS array was then molded by casting the liquid prepolymer composed of a mixture of 10:1 silicon elastomer and a curing agent (Sylgard 184). The mixture was cured at 75 °C for 4 h, and the PDMS mold was peeled from the silicon wafer. The inlet and outlet wells were punched using 3 mm diameter puncher. The molded PDMS block was then bonded to 6 well glass bottom plates (−1.5H-N, Cellvis) using oxygen-plasma treatment. The microfluidic devices were then oxygen-plasma treated and immediately coated with 1:100 (Matrigel: Expansion medium) and incubated at 37 °C and 5% $CO_2$ atmosphere for at least two hours before cell culture.

**Axotomy—**To compare MAM levels between bulk neurons and axons, we performed axotomy by physically severing the axonal chambers from the somal chambers of the

Microfluidic Two-Chamber Devices containing FAD hNPCs. The severed chambers were carefully collected in two separate conical tubes labeled as bulk neurons and axons. Protein extraction buffer was added to each tube to extract proteins from bulk neurons or axons. Equal amounts of the extracts were subjected to Western Blot analysis and probed with anti-IP3R3, anti-ACAT1 and anti-VDAC1 antibodies to determine MAM levels. To assess the purity of the axons, the extracts were also probed with antibody against nuclear envelope protein, Lamin B1 (anti-Lamin B1), present only in the nucleus of bulk neurons but not in axons. Axonal extracts showing no detectable level of Lamin B1 were considered to be pure axons.

**Compartmentalized microfluidic chambers—**To measure somal and axonal $A\beta_{40}$ we exclusively used the Xona microfluidic devices because these were able to generate fluidic separation between somal and axonal chambers. We created a thin-layer 3D culture of FAD hNPCs in these microfluidic devices to minimize contamination of soma in axonal chambers. Briefly, ~30,000 FAD hNPCs were mixed with ice-cold cell differentiation media containing BD Matrigel stock solution (1:10 dilution ratio). The mixture was immediately added to the somal chamber following the manufacturer's instruction. The chamber was transferred to 37°C for 10 min to form thin-layer (100–300 μm) 3D gels. The axonal chambers were loaded with differentiation media. Cells were allowed to differentiate for 10-days with changes of media every 3-days. We maintained a fluidic separation of 60 μL between the somal and the axonal chambers. Somal chambers contained 180 μL while the axonal chamber contained 120 μL conditioned media (CM). On the tenth day, media was exchanged with fresh media (veh) or with media containing 10 μM PRE-084 (PRE) or 10 μM NE-100 (NE). CM were collected after 16h prior to immunoblotting or Aβ-ELISA assay to determine Aβ ($A\beta_{40}$ and $A\beta_{42}$)-release. The neurons were subjected to indirect immunofluorescence analysis using anti-p-NFH or anti-tau antibodies to label axons in both axonal and somal chambers followed by confocal microscopy. Staining the nucleus with Hoechst dye determined the total number of cell bodies in somal and axonal chambers.

**ELISA and western blot—**Aβ ($A\beta_{40}$ and $A\beta_{42}$) species were measured from conditioned media of untreated or treated (PRE, CE, or BACEi-IV) Ren-GA neurons using commercially available ELISA kits from WAKO, as described before (Bhattacharyya et al., 2013, 2016). Conditioned media from the somal and axonal chambers from cells differentiated in microfluidic chambers were subjected to WAKO ELISA to measure Aβ ($A\beta_{40}$ and $A\beta_{42}$) from cell bodies and axons, respectively. $A\beta_{42}$ levels in the axonal chambers were below detectable limits, thus only axonal-$A\beta_{40}$ levels were determined. We determined the number of $A\beta_{40}$ molecules per axons or per cell body following methods described by Niederst et al. (2015). Briefly, we first calculated the amounts of total $A\beta_{40}$ release from each axonal and each somal chambers by multiplying the concentration (in μM) of $A\beta_{40}$ with total volume of conditioned media of the chambers (120 μL for axonal chamber and 150 μL for somal chamber) divided by the number of tau-positive axons per axonal chamber and Hoechst-positive soma per somal chamber. Next, we calculated the number of Aβ molecule per soma by multiplying the $A\beta_{40}$ concentrations with Avogadro's number. To calculate the number of Aβ molecules per axon, first, we multiplied $A\beta_{40}$ concentrations times Avogadro's number. Next we counted the small number of Hoechst-positive cells in the axonal chambers and

calculated the number of Aβ molecules generated from these cells as somal Aβ. This number was then subtracted from the number of Aβ molecules per axon calculated before to obtain the number of Aβ molecule per axon.

**Protein measurement—**Protein concentrations were determined by Bio Rad BCA assay. For western blot analysis samples from palmitoylation assays or from sucrose or Percol fractionation were prepared in sample buffers containing β-mercaptoethanol (βME) for denaturation. Samples were resolved on a 4%–12% gradient Bis-Tris gels (Invitrogen) prior to immunoblotting analysis using appropriate antibodies. The blots were visualized by a Li-Cor Odyssey imaging system. Band intensities were measured by ImageStudio software.

**siRNA mediated knock down—**A SMART pool siRNA (Dharmacon, Inc.) targeting four sequences within the human sigma1 receptor (S1R) transcript (CUAUUAAUAAAGAUUUGUU, CGAGUAGUGCUGCUCUUC, GGGAUAUCCAUGCUUAUGU and GUUCUAGAGUUAAGGAUGG), based on a previous report (Amer, McKeown et al., 2013). A non-targeting (si-non) siRNA was obtained as control siRNA. To knock down S1R, cells were introduced with 100nM SMART pool siRNA against S1R (si-S1R) or with the control (si-non) via electroporation technique using Amexa Mouse Neuron Nucleofector kit (Lonza) according to the manufacturer protocol. For FAD hNPCs, we used 5 X $10^6$ cells to introduce si-S1R and si-non.

**Cell viability assay—**We used CytoTox-ONE Assay (Promega) to measure cell viability. The CytoTox-ONE Assay is a rapid, fluorescent measure of the release of lactate dehydrogenase (LDH) from cells with a damaged membrane. We measured cell viability by assessing the LDH release from cells undergoing siRNA-mediated silencing, following the manufacturer's instruction. Briefly, fresh conditioned media (CM) were collected and mixed with CytoTox-ONE Reagent in a 96 well plate. The mixtures were incubated at 22°C for 10 minutes prior to adding Cyto-Tox-ONE Stop solution. LDH-release was measured by recording fluorescence (Ex = 560 nm and Em = 590 nm). Experiments were performed in triplicates. The percent cell viability was calculated by using the average fluorescence values from experimental, maximum LDH release, and culture medium background for each experiment.

### QUANTIFICATION AND STATISTICAL ANALYSIS

All statistical analyses were performed using Microsoft Excel or GraphPad Prism v.6 software (Graphpad). Exact values for experimental numbers and p values are reported in the figures and corresponding figure legends. Bars and error bars on the graphs represent mean values and SEM for multiple independent experiments as specified in each legend. Unless otherwise mentioned, statistical significances were determined by unpaired Student's t test for two groups or one-way ANOVA with Tukey's multiple comparisons test for multiple groups. All statistical analyses were performed using a two-tailed Student's t test. Data in graphs are expressed as mean values SEM $p < 0.01$ were considered significant.

## Supplementary Material

Refer to Web version on PubMed Central for supplementary material.

## ACKNOWLEDGMENTS

We thank Dr. Doo Y. Kim, Associate Professor, Massachusetts General Hospital for providing us with the 3D neural cell model of AD (FAD hNPCs); Dr. Chen Meng of Massachusetts General Hospital for help in the preparation of primary neurons; Maria Ericsson of Harvard Medical School Electron Microscopy Core facility and Diane E. Capen from MGH Center for System Biology for their help with electron microscopy; Dr. Chao Tong, Professor, Zhejiang University, China, for providing the split-GFP BiFC plasmids; and Nick Waterhouse, summer intern, for initial testing of CellLight probes in non-neuronal cells. This study was funded by grants from the NIH (5R01NS045860-19) and the Cure Alzheimer's Fund.

## REFERENCES

Amer MS, McKeown L, Tumova S, Liu R, Seymour VA, Wilson LA, Naylor J, Greenhalgh K, Hou B, Majeed Y, et al. (2013). Inhibition of endothelial cell Ca(2)(+) entry and transient receptor potential channels by Sigma-1 receptor ligands. Br. J. Pharmacol. 168, 1445–1455. [PubMed: 23121507]

Annunziata I, Patterson A, and d'Azzo A. (2013). Mitochondria-associated ER membranes (MAMs) and glycosphingolipid enriched microdomains (GEMs): isolation from mouse brain. J. Vis. Exp. (73), e50215.

Annunziata I, Sano R, and d'Azzo A. (2018). Mitochondria-associated ER membranes (MAMs) and lysosomal storage diseases. Cell Death Dis. 9, 328. [PubMed: 29491402]

Area-Gomez E, de Groof AJ, Boldogh I, Bird TD, Gibson GE, Koehler CM, Yu WH, Duff KE, Yaffe MP, Pon LA, and Schon EA (2009). Pre-senilins are enriched in endoplasmic reticulum membranes associated with mitochondria. Am. J. Pathol. 175, 1810–1816. [PubMed: 19834068]

Area-Gomez E, Del Carmen Lara Castillo M, Tambini MD, Guardia-Laguarta C, de Groof AJ, Madra M, Ikenouchi J, Umeda M, Bird TD, Sturley SL, and Schon EA (2012). Upregulated function of mitochondria-associated ER membranes in Alzheimer disease. EMBO J. 31, 4106–4123. [PubMed: 22892566]

Bannai H, Inoue T, Nakayama T, Hattori M, and Mikoshiba K. (2004). Kinesin dependent, rapid, bi-directional transport of ER sub-compartment in dendrites of hippocampal neurons. J. Cell Sci. 117, 163–175. [PubMed: 14676272]

Bernard-Marissal N, Médard JJ, Azzedine H, and Chrast R. (2015). Dysfunction in endoplasmic reticulum-mitochondria crosstalk underlies SIG-MAR1 loss of function mediated motor neuron degeneration. Brain 138, 875–890. [PubMed: 25678561]

Bhattacharyya R, and Kovacs DM (2010). ACAT inhibition and amyloid beta reduction. Biochim. Biophys. Acta 1801, 960–965. [PubMed: 20398792]

Bhattacharyya R, Barren C, and Kovacs DM (2013). Palmitoylation of amyloid precursor protein regulates amyloidogenic processing in lipid rafts. J. Neurosci. 33, 11169–11183. [PubMed: 23825420]

Bhattacharyya R, Fenn RH, Barren C, Tanzi RE, and Kovacs DM (2016). Palmitoylated APP Forms Dimers, Cleaved by BACE1. PLoS ONE 11, e0166400.

Brendza RP, Simmons K, Bales KR, Paul SM, Goldberg MP, and Holtzman DM (2003). Use of YFP to study amyloid-beta associated neurite alterations in live brain slices. Neurobiol. Aging 24, 1071–1077. [PubMed: 14643378]

Bryleva EY, Rogers MA, Chang CC, Buen F, Harris BT, Rousselet E, Seidah NG, Oddo S, LaFerla FM, Spencer TA, et al. (2010). ACAT1 gene ablation increases 24(S)-hydroxycholesterol content in the brain and ameliorates amyloid pathology in mice with AD. Proc. Natl. Acad. Sci. USA 107, 3081–3086. [PubMed: 20133765]

Buxbaum JD, Thinakaran G, Koliatsos V, O'Callahan J, Slunt HH, Price DL, and Sisodia SS (1998). Alzheimer amyloid protein precursor in the rat hippocampus: transport and processing through the perforant path. J. Neurosci. 18, 9629–9637. [PubMed: 9822724]

Chevalier-Larsen E, and Holzbaur EL (2006). Axonal transport and neurodegenerative disease. Biochim. Biophys. Acta 1762, 1094–1108. [PubMed: 16730956]

Choi SH, Kim YH, Hebisch M, Sliwinski C, Lee S, D'Avanzo C, Chen H, Hooli B, Asselin C, Muffat J, et al. (2014). A three-dimensional human neural cell culture model of Alzheimer's disease. Nature 515, 274–278. [PubMed: 25307057]

Cirrito JR, Yamada KA, Finn MB, Sloviter RS, Bales KR, May PC, Schoepp DD, Paul SM, Mennerick S, and Holtzman DM (2005). Synaptic activity regulates interstitial fluid amyloid-beta levels in vivo. Neuron 48, 913–922. [PubMed: 16364896]

Cirrito JR, Kang JE, Lee J, Stewart FR, Verges DK, Silverio LM, Bu G, Mennerick S, and Holtzman DM (2008). Endocytosis is required for synaptic activity-dependent release of amyloid-beta in vivo. Neuron 58, 42–51. [PubMed: 18400162]

Cleary JP, Walsh DM, Hofmeister JJ, Shankar GM, Kuskowski MA, Selkoe DJ, and Ashe KH (2005). Natural oligomers of the amyloid-beta pro- tein specifically disrupt cognitive function. Nat. Neurosci. 8, 79–84. [PubMed: 15608634]

Cross DJ, Flexman JA, Anzai Y, Maravilla KR, and Minoshima S. (2008). Age-related decrease in axonal transport measured by MR imaging in vivo. Neuroimage 39, 915–926. [PubMed: 17980625]

D'Avanzo C, Aronson J, Kim YH, Choi SH, Tanzi RE, and Kim DY (2015). Alzheimer's in 3D culture: challenges and perspectives. BioEssays 37, 1139–1148. [PubMed: 26252541]

Dai CL, Shi J, Chen Y, Iqbal K, Liu F, and Gong CX (2013). Inhibition of protein synthesis alters protein degradation through activation of protein kinase B (AKT). J. Biol. Chem. 288, 23875–23883. [PubMed: 23843462]

Das U, Scott DA, Ganguly A, Koo EH, Tang Y, and Roy S. (2013). Activity-induced convergence of APP and BACE-1 in acidic microdomains via an endocytosis-dependent pathway. Neuron 79, 447–460. [PubMed: 23931995]

Das U, Wang L, Ganguly A, Saikia JM, Wagner SL, Koo EH, and Roy S. (2016). Visualizing APP and BACE-1 approximation in neurons yields insight into the amyloidogenic pathway. Nat. Neurosci. 19, 55–64. [PubMed: 26642089]

Erpapazoglou Z, Mouton-Liger F, and Corti O. (2017). From dysfunctional endoplasmic reticulum-mitochondria coupling to neurodegeneration. Neurochem. Int. 109, 171–183. [PubMed: 28389271]

Filadi R, Greotti E, Turacchio G, Luini A, Pozzan T, and Pizzo P. (2015). Mitofusin 2 ablation increases endoplasmic reticulum-mitochondria coupling. Proc. Natl. Acad. Sci. USA 112, E2174–E2181. [PubMed: 25870285]

Giorgi C, De Stefani D, Bononi A, Rizzuto R, and Pinton P. (2009). Structural and functional link between the mitochondrial network and the endoplasmic reticulum. Int. J. Biochem. Cell Biol. 41, 1817–1827. [PubMed: 19389485]

Haass C, and Selkoe DJ (2007). Soluble protein oligomers in neurodegeneration: lessons from the Alzheimer's amyloid beta-peptide. Nat. Rev. Mol. Cell Biol. 8, 101–112. [PubMed: 17245412]

Haass C, Lemere CA, Capell A, Citron M, Seubert P, Schenk D, Lannfelt L, and Selkoe DJ (1995). The Swedish mutation causes early-onset Alz- heimer's disease by β-secretase cleavage within the secretory pathway. Nat. Med. 1, 1291–1296. [PubMed: 7489411]

Hajnóczky G, Csordás G, Das S, Garcia-Perez C, Saotome M, Sinha Roy S, and Yi M. (2006). Mitochondrial calcium signalling and cell death: approaches for assessing the role of mitochondrial Ca2+ uptake in apoptosis. Cell Calcium 40, 553–560. [PubMed: 17074387]

Hayashi T, and Su TP (2007). Sigma-1 receptor chaperones at the ER-mitochondrion interface regulate Ca(2+) signaling and cell survival. Cell 131, 596–610. [PubMed: 17981125]

Hedskog L, Pinho CM, Filadi R, Rönnbäck A, Hertwig L, Wiehager B, Larssen P, Gellhaar S, Sandebring A, Westerlund M, et al. (2013). Modulation of the endoplasmic reticulum-mitochondria interface in Alzheimer's disease and related models. Proc. Natl. Acad. Sci. USA 110, 7916–7921. [PubMed: 23620518]

Hutter-Paier B, Huttunen HJ, Puglielli L, Eckman CB, Kim DY, Hofmeister A, Moir RD, Domnitz SB, Frosch MP, Windisch M, and Kovacs DM (2004). The ACAT inhibitor CP-113,818 markedly reduces amyloid pathology in a mouse model of Alzheimer's disease. Neuron 44, 227–238. [PubMed: 15473963]

Huttunen HJ, Greco C, and Kovacs DM (2007). Knockdown of ACAT-1 reduces amyloidogenic processing of APP. FEBS Lett. 581, 1688–1692. [PubMed: 17412327]

Huttunen HJ, Peach C, Bhattacharyya R, Barren C, Pettingell W, Hutter-Paier B, Windisch M, Berezovska O, and Kovacs DM (2009). Inhibition of acyl-coenzyme A: cholesterol acyl

transferase modulates amyloid precursor protein trafficking in the early secretory pathway. FASEB J. 23, 3819–3828. [PubMed: 19625658]

Huttunen HJ, Havas D, Peach C, Barren C, Duller S, Xia W, Frosch MP, Hutter-Paier B, Windisch M, and Kovacs DM (2010). The acyl-coenzyme A: cholesterol acyltransferase inhibitor CI-1011 reverses diffuse brain amyloid pathology in aged amyloid precursor protein transgenic mice. J. Neuropathol. Exp. Neurol. 69, 777–788. [PubMed: 20613640]

Kaether C, Skehel P, and Dotti CG (2000). Axonal membrane proteins are transported in distinct carriers: a two-color video microscopy study in cultured hippocampal neurons. Mol. Biol. Cell 11, 1213–1224. [PubMed: 10749925]

Kamal A, Almenar-Queralt A, LeBlanc JF, Roberts EA, and Goldstein LS (2001). Kinesin-mediated axonal transport of a membrane compartment containing beta-secretase and presenilin-1 requires APP. Nature 414, 643–648. [PubMed: 11740561]

Kanaan NM, Pigino GF, Brady ST, Lazarov O, Binder LI, and Morfini GA (2013). Axonal degeneration in Alzheimer's disease: when signaling abnormalities meet the axonal transport system. Exp. Neurol. 246, 44–53. [PubMed: 22721767]

Kim YH, Choi SH, D'Avanzo C, Hebisch M, Sliwinski C, Bylykbashi E, Washicosky KJ, Klee JB, Brüstle O, Tanzi RE, and Kim DY (2015). A 3D human neural cell culture system for modeling Alzheimer's disease. Nat. Protoc. 10, 985–1006. [PubMed: 26068894]

Koo EH, Sisodia SS, Archer DR, Martin LJ, Weidemann A, Beyreuther K, Fischer P, Masters CL, and Price DL (1990). Precursor of amyloid protein in Alzheimer disease undergoes fast anterograde axonal transport. Proc. Natl. Acad. Sci. USA 87, 1561–1565. [PubMed: 1689489]

Koo EH, Squazzo SL, Selkoe DJ, and Koo CH (1996). Trafficking of cell-surface amyloid β-protein precursor. I. Secretion, endocytosis and recycling as detected by labeled monoclonal antibody. J. Cell Sci. 109, 991–998. [PubMed: 8743946]

Koppensteiner P, Trinchese F, Fà M, Puzzo D, Gulisano W, Yan S, Poussin A, Liu S, Orozco I, Dale E, et al. (2016). Time-dependent reversal of synaptic plasticity induced by physiological concentrations of oligomeric Ab42: an early index of Alzheimer's disease. Sci. Rep. 6, 32553. [PubMed: 27581852]

Kosicek M, Malnar M, Goate A, and Hecimovic S. (2010). Cholesterol accumulation in Niemann Pick type C (NPC) model cells causes a shift in APP localization to lipid rafts. Biochem. Biophys. Res. Commun. 393, 404–409. [PubMed: 20138836]

Kwak SS, Washicosky KJ, Brand E, von Maydell D, Aronson J, Kim S, Capen DE, Cetinbas M, Sadreyev R, Ning S, et al. (2020). Amyloid-β42/40 ratio drives tau pathology in 3D human neural cell culture models of Alzheimer's disease. Nat. Commun. 11, 1377. [PubMed: 32170138]

Kwart D, Gregg A, Scheckel C, Murphy EA, Paquet D, Duffield M, Fak J, Olsen O, Darnell RB, and Tessier-Lavigne M. (2019). A Large Panel of Isogenic APP and PSEN1 Mutant Human iPSC Neurons Reveals Shared Endosomal Abnormalities Mediated by APP β-CTFs, Not Aβ. Neuron 104, 1022. [PubMed: 31805257]

Lazarov O, Lee M, Peterson DA, and Sisodia SS (2002). Evidence that synaptically released beta-amyloid accumulates as extracellular deposits in the hippocampus of transgenic mice. J. Neurosci. 22, 9785–9793. [PubMed: 12427834]

Leal NS, Schreiner B, Pinho CM, Filadi R, Wiehager B, Karlström H, Pizzo P, and Ankarcrona M. (2016). Mitofusin-2 knockdown increases ER-mitochondria contact and decreases amyloid β-peptide production. J. Cell. Mol. Med. 20, 1686–1695. [PubMed: 27203684]

Lee EB, Zhang B, Liu K, Greenbaum EA, Doms RW, Trojanowski JQ, and Lee VM (2005). BACE overexpression alters the subcellular processing of APP and inhibits Abeta deposition in vivo. J. Cell Biol. 168, 291–302. [PubMed: 15642747]

Lee S, Wang W, Hwang J, Namgung U, and Min KT (2019). Increased ER-mitochondria tethering promotes axon regeneration. Proc. Natl. Acad. Sci. USA 116, 16074–16079. [PubMed: 31332012]

Lewin TM, Van Horn CG, Krisans SK, and Coleman RA (2002). Rat liver acyl-CoA synthetase 4 is a peripheral-membrane protein located in two distinct subcellular organelles, peroxisomes, and mitochondrial-associated membrane. Arch. Biochem. Biophys. 404, 263–270. [PubMed: 12147264]

Linder ME, and Deschenes RJ (2007). Palmitoylation: policing protein stability and traffic. Nat. Rev. Mol. Cell Biol. 8, 74–84. [PubMed: 17183362]

Liu Y, Ma X, Fujioka H, Liu J, Chen S, and Zhu X. (2019). DJ-1 regulates the integrity and function of ER-mitochondria association through interaction with IP3R3-Grp75-VDAC1. Proc. Natl. Acad. Sci. USA 116, 25322–25328. [PubMed: 31767755]

Lomoio S, Willen R, Kim W, Ho KZ, Robinson EK, Prokopenko D, Kennedy ME, Tanzi RE, and Tesco G. (2020). Gga3 deletion and a GGA3 rare variant associated with late onset Alzheimer's disease trigger BACE1 accumulation in axonal swellings. Sci. Transl. Med. 12, eaba1871.

Lorenzen A, Samosh J, Vandewark K, Anborgh PH, Seah C, Magal- haes AC, Cregan SP, Ferguson SS, and Pasternak SH (2010). Rapid and direct transport of cell surface APP to the lysosome defines a novel selective pathway. Mol. Brain 3, 11. [PubMed: 20409323]

Macaskill AF, Rinholm JE, Twelvetrees AE, Arancibia-Carcamo IL, Muir J, Fransson A, Aspenstrom P, Attwell D, and Kittler JT (2009). Miro1 is a calcium sensor for glutamate receptor-dependent localization of mitochondria at synapses. Neuron 61, 541–555. [PubMed: 19249275]

Mango D, Saidi A, Cisale GY, Feligioni M, Corbo M, and Nisticò R. (2019). Targeting Synaptic Plasticity in Experimental Models of Alzheimer's Disease. Front. Pharmacol. 10, 778. [PubMed: 31379566]

Martino Adami PV, Nichtová Z, Weaver DB, Bartok A, Wisniewski T, Jones DR, Do Carmo S, Castaño EM, Cuello AC, Hajnóczky G, and Morelli L. (2019). Perturbed mitochondria-ER contacts in live neurons that model the amyloid pathology of Alzheimer's disease. J. Cell Sci. 132, jcs229906.

Merianda TT, Lin AC, Lam JS, Vuppalanchi D, Willis DE, Karin N, Holt CE, and Twiss JL (2009). A functional equivalent of endoplasmic reticulum and Golgi in axons for secretion of locally synthesized proteins. Mol. Cell. Neurosci. 40, 128–142. [PubMed: 19022387]

Misko A, Jiang S, Wegorzewska I, Milbrandt J, and Baloh RH (2010). Mitofusin 2 is necessary for transport of axonal mitochondria and interacts with the Miro/Milton complex. J. Neurosci. 30, 4232–4240. [PubMed: 20335458]

Muresan V, Varvel NH, Lamb BT, and Muresan Z. (2009). The cleavage products of amyloid-beta precursor protein are sorted to distinct carrier vesicles that are independently transported within neurites. J. Neurosci. 29, 3565–3578. [PubMed: 19295161]

Murphy SR, Chang CC, Dogbevia G, Bryleva EY, Bowen Z, Hasan MT, and Chang TY (2013). Acat1 knockdown gene therapy decreases amyloid-β in a mouse model of Alzheimer's disease. Mol. Ther. 21, 1497–1506. [PubMed: 23774792]

Niederst ED, Reyna SM, and Goldstein LS (2015). Axonal amyloid precursor protein and its fragments undergo somatodendritic endocytosis and processing. Mol. Biol. Cell 26, 205–217. [PubMed: 25392299]

Pera M, Larrea D, Guardia-Laguarta C, Montesinos J, Velasco KR, Agrawal RR, Xu Y, Chan RB, Di Paolo G, Mehler MF, et al. (2017). Increased localization of APP-C99 in mitochondria-associated ER membranes causes mitochondrial dysfunction in Alzheimer disease. EMBO J. 36, 3356–3371. [PubMed: 29018038]

Peric A, and Annaert W. (2015). Early etiology of Alzheimer's disease: tipping the balance toward autophagy or endosomal dysfunction? Acta Neuropathol. 129, 363–381. [PubMed: 25556159]

Pizzo P, and Pozzan T. (2007). Mitochondria-endoplasmic reticulum choreography: structure and signaling dynamics. Trends Cell Biol. 17, 511–517. [PubMed: 17851078]

Poston CN, Krishnan SC, and Bazemore-Walker CR (2013). In-depth proteomic analysis of mammalian mitochondria-associated membranes (MAM). J. Proteomics 79, 219–230. [PubMed: 23313214]

Puglielli L, Konopka G, Pack-Chung E, Ingano LAM, Berezovska O, Hyman BT, Chang TY, Tanzi RE, and Kovacs DM (2001). Acyl-coenzyme A: cholesterol acyltransferase modulates the generation of the amyloid beta- peptide. Nat. Cell Biol. 3, 905–912. [PubMed: 11584272]

Qin D, Xia Y, and Whitesides GM (2010). Soft lithography for micro- and nanoscale patterning. Nat. Protoc. 5, 491–502. [PubMed: 20203666]

Rowland AA, and Voeltz GK (2012). Endoplasmic reticulum-mitochondria contacts: function of the junction. Nat. Rev. Mol. Cell Biol. 13, 607–625. [PubMed: 22992592]

Rusiñol AE, Cui Z, Chen MH, and Vance JE (1994). A unique mitochondria-associated membrane fraction from rat liver has a high capacity for lipid synthesis and contains pre-Golgi secretory proteins including nascent lipoproteins. J. Biol. Chem. 269, 27494–27502. [PubMed: 7961664]

Ryskamp DA, Korban S, Zhemkov V, Kraskovskaya N, and Bezprozvanny I. (2019). Neuronal Sigma-1 Receptors: Signaling Functions and Protective Roles in Neurodegenerative Diseases. Front. Neurosci. 13, 862. [PubMed: 31551669]

Sala-Vila A, Navarro-Lérida I, Sánchez-Alvarez M, Bosch M, Calvo C, López JA, Calvo E, Ferguson C, Giacomello M, Serafini A, et al. (2016). Interplay between hepatic mitochondria-associated membranes, lipid metabolism and caveolin-1 in mice. Sci. Rep. 6, 27351. [PubMed: 27272971]

Sannerud R, Declerck I, Peric A, Raemaekers T, Menendez G, Zhou L, Veerle B, Coen K, Munck S, De Strooper B, et al. (2011). ADP ribosylation factor 6 (ARF6) controls amyloid precursor protein (APP) processing by mediating the endosomal sorting of BACE1. Proc. Natl. Acad. Sci. USA 108, E559–E568. [PubMed: 21825135]

Schon EA, and Area-Gomez E. (2013). Mitochondria-associated ER membranes in Alzheimer disease. Mol. Cell. Neurosci. 55, 26–36. [PubMed: 22922446]

Schreiner B, Hedskog L, Wiehager B, and Ankarcrona M. (2015). Amyloid-β peptides are generated in mitochondria-associated endoplasmic reticulum membranes. J. Alzheimers Dis. 43, 369–374. [PubMed: 25096627]

Serrano-Pozo A, Frosch MP, Masliah E, and Hyman BT (2011). Neuropathological alterations in Alzheimer disease. Cold Spring Harb. Perspect. Med. 1, a006189.

Sheng JG, Price DL, and Koliatsos VE (2002). Disruption of corticocortical connections ameliorates amyloid burden in terminal fields in a transgenic model of Abeta amyloidosis. J. Neurosci. 22, 9794–9799. [PubMed: 12427835]

Shibuya Y, Niu Z, Bryleva EY, Harris BT, Murphy SR, Kheirollah A, Bowen ZD, Chang CCY, and Chang TY (2015). Acyl-coenzyme A:cholesterol acyltransferase 1 blockage enhances autophagy in the neurons of triple transgenic Alzheimer's disease mouse and reduces human P301L-tau content at the presymptomatic stage. Neurobiol. Aging 36, 2248–2259. [PubMed: 25930235]

Simons VM (1995). [Molecular mechanisms in Alzheimer disease]. Fortschr. Med. 113, 441–442. [PubMed: 8529982]

Sisodia SS, Koo EH, Hoffman PN, Perry G, and Price DL (1993). Identification and transport of full-length amyloid precursor proteins in rat peripheral nervous system. J. Neurosci. 13, 3136–3142. [PubMed: 8331390]

Spires TL, Meyer-Luehmann M, Stern EA, McLean PJ, Skoch J, Nguyen PT, Bacskai BJ, and Hyman BT (2005). Dendritic spine abnormalities in amyloid precursor protein transgenic mice demonstrated by gene transfer and intravital multiphoton microscopy. J. Neurosci. 25, 7278–7287. [PubMed: 16079410]

Stokin GB, Lillo C, Falzone TL, Brusch RG, Rockenstein E, Mount SL, Raman R, Davies P, Masliah E, Williams DS, and Goldstein LS (2005). Axonopathy and transport deficits early in the pathogenesis of Alzheimer's disease. Science 307, 1282–1288. [PubMed: 15731448]

Suo Z, Wu M, Citron BA, Wong GT, and Festoff BW (2004). Abnormality of G-protein-coupled receptor kinases at prodromal and early stages of Alzheimer's disease: an association with early beta-amyloid accumulation. J. Neurosci. 24, 3444–3452. [PubMed: 15056724]

Szymański J, Janikiewicz J, Michalska B, Patalas-Krawczyk P, Perrone M, Ziółkowski W, Duszyński J, Pinton P, Dobrzyń A, and Więckowski MR (2017). Interaction of Mitochondria with the Endoplasmic Reticulum and Plasma Membrane in Calcium Homeostasis, Lipid Trafficking and Mitochondrial Structure. Int. J. Mol. Sci. 18, E1576. [PubMed: 28726733]

Tampellini D, Rahman N, Gallo EF, Huang Z, Dumont M, Capetillo-Zarate E, Ma T, Zheng R, Lu B, Nanus DM, et al. (2009). Synaptic activity reduces intraneuronal Abeta, promotes APP transport to synapses, and protects against Abeta-related synaptic alterations. J. Neurosci. 29, 9704–9713. [PubMed: 19657023]

Taylor AM, Blurton-Jones M, Rhee SW, Cribbs DH, Cotman CW, and Jeon NL (2005). A microfluidic culture platform for CNS axonal injury, regen- eration and transport. Nat. Methods 2, 599–605. [PubMed: 16094385]

Teipel SJ, Stahl R, Dietrich O, Schoenberg SO, Perneczky R, Bokde AL, Reiser MF, Möller HJ, and Hampel H. (2007). Multivariate network analysis of fiber tract integrity in Alzheimer's disease. Neuroimage 34, 985–995. [PubMed: 17166745]

Urano Y, Hayashi I, Isoo N, Reid PC, Shibasaki Y, Noguchi N, Tomita T, Iwatsubo T, Hamakubo T, and Kodama T. (2005). Association of active gamma-secretase complex with lipid rafts. J. Lipid Res. 46, 904–912. [PubMed: 15716592]

Vetrivel KS, Cheng H, Kim SH, Chen Y, Barnes NY, Parent AT, Sisodia SS, and Thinakaran G. (2005). Spatial segregation of gamma-secretase and substrates in distinct membrane domains. J. Biol. Chem. 280, 25892–25900. [PubMed: 15886206]

Vetrivel KS, Meckler X, Chen Y, Nguyen PD, Seidah NG, Vassar R, Wong PC, Fukata M, Kounnas MZ, and Thinakaran G. (2009). Alzheimer disease Abeta production in the absence of S-palmitoylation-dependent targeting of BACE1 to lipid rafts. J. Biol. Chem. 284, 3793–3803. [PubMed: 19074428]

Volpe P, Villa A, Damiani E, Sharp AH, Podini P, Snyder SH, and Meldolesi J. (1991). Heterogeneity of microsomal Ca2+ stores in chicken Purkinje neurons. EMBO J. 10, 3183–3189. [PubMed: 1915290]

Wang X, and Schwarz TL (2009). The mechanism of Ca2+ -dependent regulation of kinesin-mediated mitochondrial motility. Cell 136, 163–174. [PubMed: 19135897]

Wieckowski MR, Giorgi C, Lebiedzinska M, Duszynski J, and Pinton P. (2009). Isolation of mitochondria-associated membranes and mitochondria from animal tissues and cells. Nat. Protoc. 4, 1582–1590. [PubMed: 19816421]

Yamazaki T, Selkoe DJ, and Koo EH (1995). Trafficking of cell surface β-amyloid precursor protein: retrograde and transcytotic transport in cultured neurons. J. Cell Biol. 129, 431–442. [PubMed: 7721945]

Yang Z, Zhao X, Xu J, Shang W, and Tong C. (2018). A novel fluorescent reporter detects plastic remodeling of mitochondria-ER contact sites. J. Cell Sci. 131, jcs208686.

Yu W, Jin H, and Huang Y. (2021). Mitochondria-associated membranes (MAMs): a potential therapeutic target for treating Alzheimer's disease. Clin. Sci. (Lond.) 135, 109–126. [PubMed: 33404051]

## Highlights

- Palmitoylated APP (*pal*APP) is enriched in mitochondrial-associated ER membranes (MAMs)
- Upregulation of MAM increases cell surface *pal*APP levels and axonal Aβ generation
- Downregulation of MAM attenuates cell surface *pal*APP levels and axonal Aβ generation

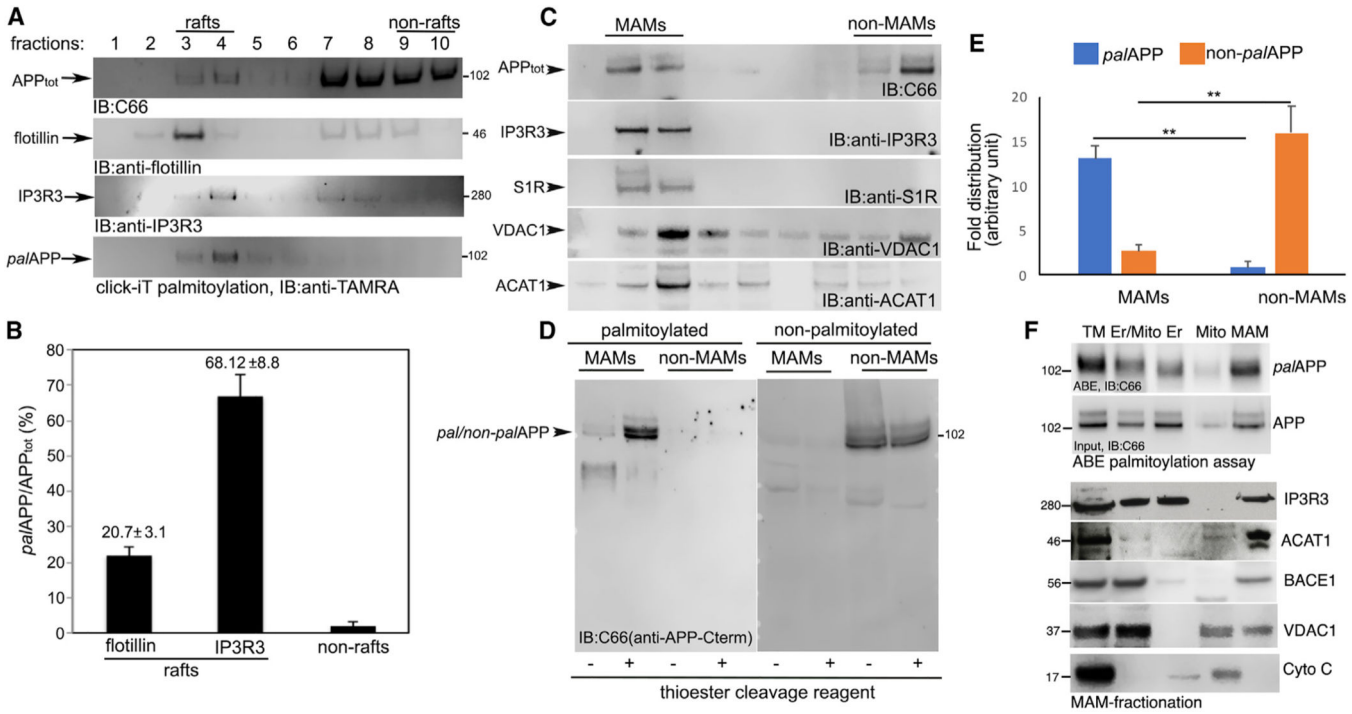


**Figure 1. palAPP is predominantly distributed in the ER-rafts or MAMs in differentiated human stem cell-derived neural progenitor FAD-NPC neurons and in mouse brain**

(A) FAD hNPCs were plated on a thin-layer 3D matrix prior to differentiation. Lipid rafts and non-raft fractionation of 10-day differentiated FAD hNPCs pre-labeled with reactive alkylene-palmitic acid (alkyl-C16) prior to western blot analysis. First, second, and third blots: detection of total APP ($APP_{tot}$) by probing with anti-APP C-terminal antibody (C66), detection of rafts by probing with anti-flotillin, or anti-IP3R3 antibodies, respectively. Fourth blot: detection of palmitic acid labeled APP (palAPP) after TAMRA (tetramethylrhodamine)-labeling via click-iT reaction and probing with anti-TAMRA antibody.

(B) Quantitation of palAPP in flotillin- and IP3R3-positive fractions shown in (A) normalized to $APP_{tot}$. Data represent Mean ± SEM ($n = 3$, $p < 0.004$).

(C) Fractionations of MAMs and non-MAMs from crude ER-mitochondria membranes isolated from FAD-NPCs. Fractions were probed for indicated proteins.

(D) Badrilla palmitoylation assay to isolate palmitoylated and non-palmitoylated proteins from MAM and non-MAM fractions isolated in (C).

(E) Quantitation of palAPP and non-palAPP in MAMs and non-MAMs. Data represent Mean ± SEM ($n = 3$, $p < 0.01$).

(F) MAM-fractionation of total membrane extract (TM) from mouse brain via sequential extraction and Percoll gradient centrifugation to isolate crude ER- mitochondria (ER/mito), pure mitochondria (mito), and pure MAMs. Fractions were subjected to ABE palmitoylation assay followed by probing total APP (input) and ABE isolated palAPP (ABE) in each fraction with anti-APP(C-term) antibody (IB: C66). Fractions were probed with indicated antibodies. IP3R3 and ACAT1 partitioned in the MAMs. VDAC1 partitioned in both mito and MAMs. Cyto C was detected exclusively in the mito fractions. Representative image of two separate and independent experiments.

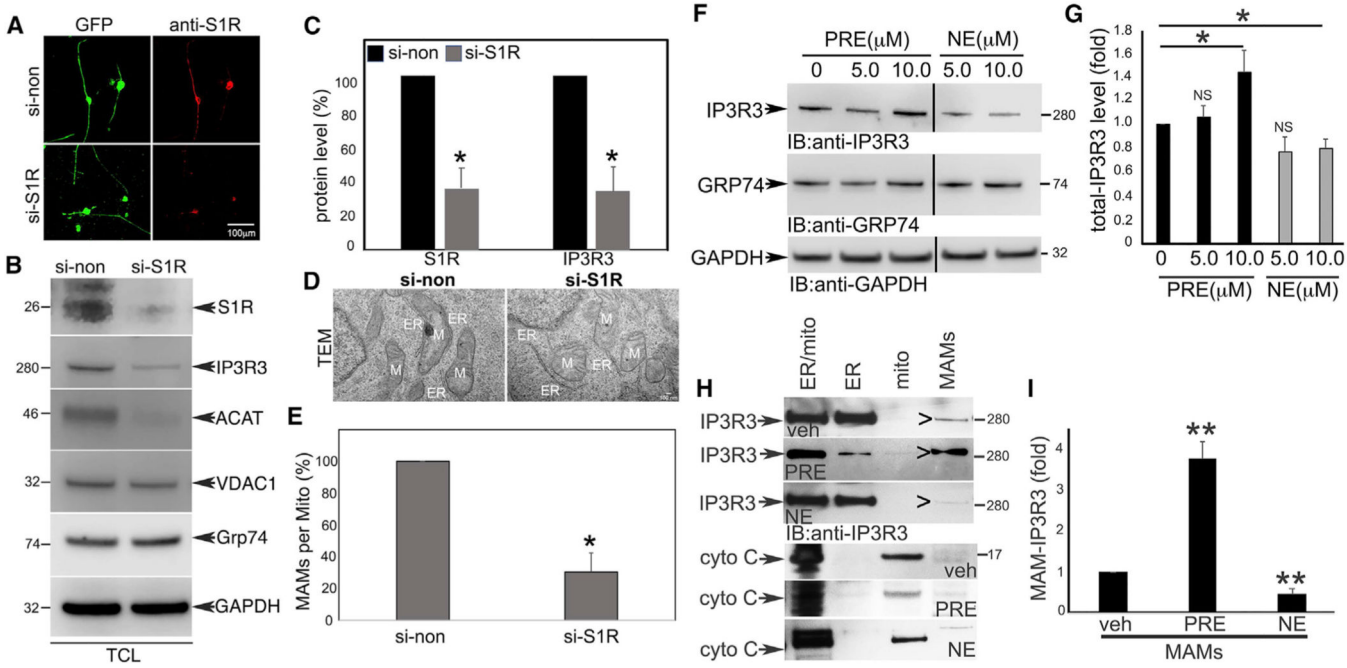


**Figure 2. Silencing or inactivation of MAM-resident sigma-1 receptor (S1R) in FAD hNPCs decreases MAM levels and reduces palAPP level and sAPPβ release**

(A) Representative confocal microscopic images of FAD hNPCs after silencing of sigma1 receptor (S1R) expression. Cells were either introduced with a non-targeting siRNA (si-non) or with a SMART pool of siRNAs against human sigma1 receptor gene Sigmar1 (si-S1R) for 48 h. Left: GFP-expressing (green) FAD NPCs containing si-non or si-S1R. Right: endogenous S1R (red) expression in cells containing si-non or si-S1R.

(B) Representative immunoblots of cell lysates (TCL) from FAD NPCs containing si-non or si-S1R probed with indicated antibodies.

(C) Quantitative analysis of S1R and IP3R3 levels from 3B. Data were analyzed using ImageJ and expressed as fold ± SEM relative to control (si-non) (n = 3, *p < 0.005).

(D) Representative electron micrographs (EM) showing ER (ER)-mitochondria (M) contact sites or MAMs (arrowheads) in FAD NPCs containing si-non or si-S1R for 48 h.

(E) Quantitation of MAMs in control (si-non) and S1R-silenced (si-S1R) cells per mitochondria per frame (MAM per M). More than 8 frames were used for each analysis (n = 3, *p < 0.01).

(F) Immunoblot of FAD NPCs treated with increasing amounts of S1R agonist PRE-084 or with S1R antagonist NE-100. MAM levels were identified by probing with antibody against MAM-protein IP3R3 (IB:anti-IP3R3). Levels of mitochondrial protein GRP74 or housekeeping protein GAPDH were detected by probing with anti-GRP74 or anti-GAPDH antibodies, respectively.

(G) Quantitative analyses of IP3R3 levels from untreated (0 μM), PRE- (5 and 10 μM), or NE- (5 and 10 μM) treated cells. IP3R3 levels were presented as fold ± SEM (n = 3, *p < 0.01).

(H) Immunoblots of pure MAM fractions (MAMs) isolated from crude ER/mitochondria (ER/mito) of FAD hNPCs after treatment with control vehicle (veh) or with 10 μM PRE or NE for 16 h. Crude ER-mitochondria extracts (ER/mito), pure ER (ER), pure mitochondria

(mito), and pure MAM (MAMs) fractions were probed with antibodies against MAM-resident IP3R3 or with mitochondrial marker Cyto C. Representative image of a triplicate experiments was presented.

(I) Quantitation of the IP3R3 levels in the MAMs from control (veh), PRE- or NE-treated cells. The levels were represented as fold ± SEM.

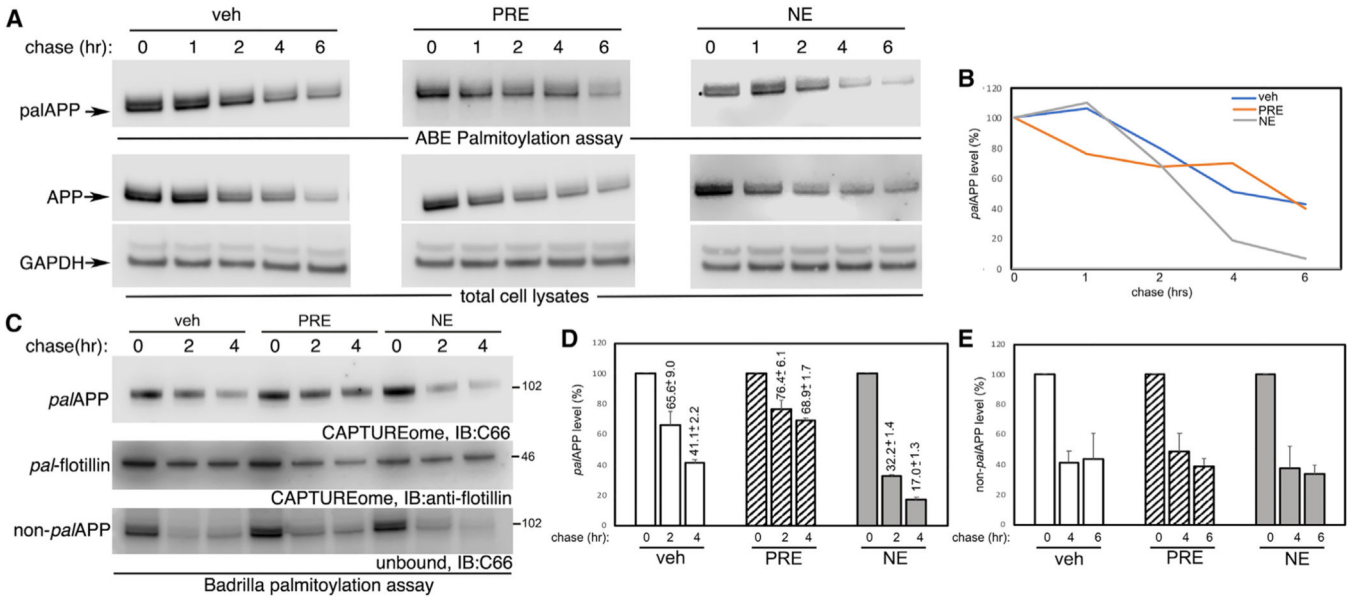


**Figure 3. Activation or inactivation of S1R specifically increases or decreases palAPP stability, respectively**

(A–E) FAD-NPCs were subjected to cycloheximide chase analysis followed by ABE (A and B) or Badrilla (C–E) palmitoylation assays to determine half-life of *pal*APP in absence or presence of S1R agonist/antagonist.

(A) ABE palmitoylation assay of FAD NPCs pre-treated without (veh) or with 10 μM PRE-084 (PRE) or NE-100 (NE) prior to cycloheximide (CHX) chase for indicated time intervals (0–18 h) revealed an increased half-life of *pal*APP in the presence of PRE and a decreased half-life of *pal*APP in the presence of NE in comparison to untreated (veh) cells (ABE palmitoylation assay). Half-life of total APP ($APP_{tot}$) remained unaltered in presence of PRE or NE.

(B) Quantitative analysis of *pal*APP/$APP_{tot}$ after cycloheximide chase in absence (veh) or presence of PRE or NE (n = 3).

(C) Representative western blots of Badrilla palmitoylation assay detecting palmitoylated APP (*pal*APP) (CAPTUREome, IP:C66) and non-palmitoylated APP (non-*pal*APP) (unbound, IB:C66) from cells chased with CHX for 0, 4, and 6 h in absence (veh) or presence of PRE and NE.

(D) Quantitation of *pal*APP/$APP_{tot}$ in absence (veh) or presence of PRE or NE after CHX-chase.

(E) Quantitation of non-*pal*APP/$APP_{tot}$. Error bars represent percent (%) ± SEM (n = 3).

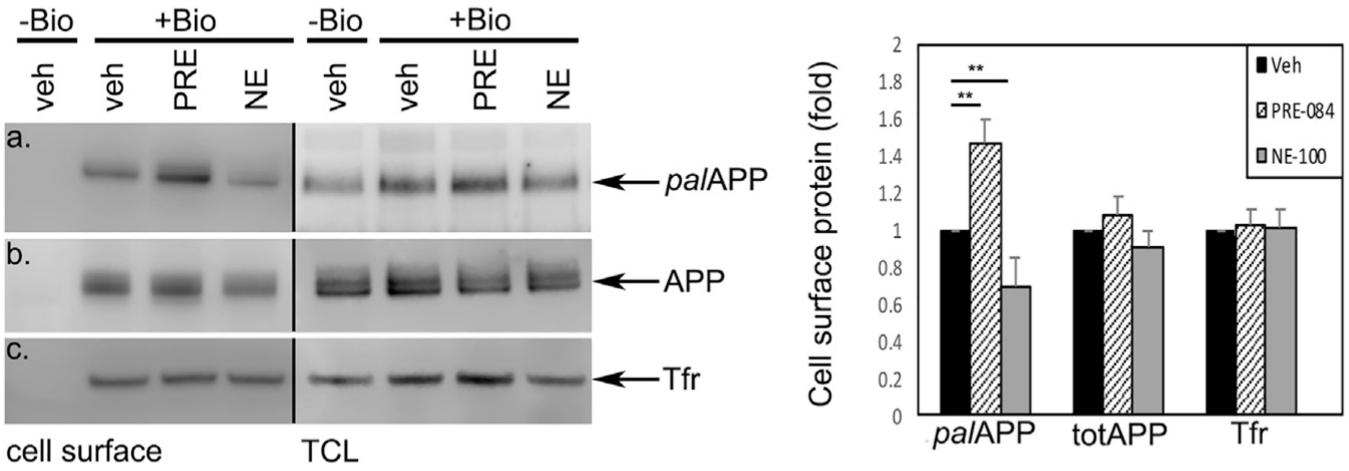


**Figure 4. Activation or inactivation of S1R specifically increases or decreases cell surface association of palAPP, respectively**

(A) Badrilla palmitoylation assay of biotinylated cell surface proteins of FAD NPCs pre-treated without (+veh) or with PRE-084 (PRE) or NE-100 (NE). Left panels (a–c): western blot detecting increased or decreased cell surface *pal*APP in presence of PRE or NE, respectively, in comparison to untreated (veh) cells (a). Cell surface total APP ($APP_{tot}$) and flotillin are represented in b and c. Right panel: representative western blot images of *pal*APP, $APP_{tot}$, or flotillin in total cell lysates from untreated (veh), PRE- or NE-treated cells.

(B) Quantitation showed ~1.5-fold increase of cell surface *pal*APP after activation of S1R by PRE-treatment, whereas inactivation of S1R by NE-treatment significantly decreased cell surface *pal*APP level. Neither PRE- nor NE-treatment had any significant effect on cell surface association of either non-*pal*APP or Tfr. Error bars are fold ± SEM (n = 2, **$p < 0.05$).

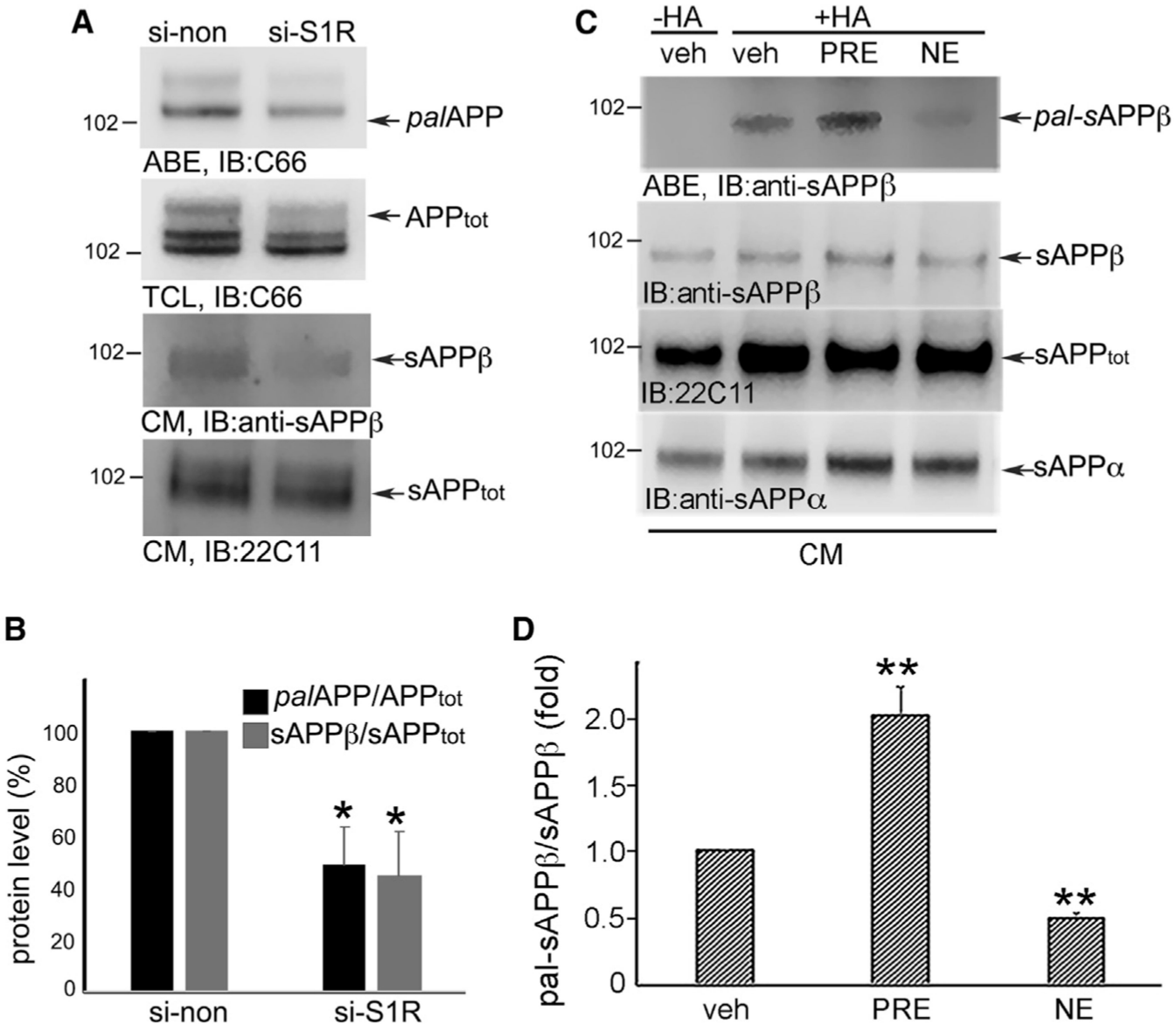


**Figure 5. Silencing of S1R and modulation of S1R-activity regulates β-secretase cleavage of APP and palAPP, respectively**

(A) Upper panel: ABE palmitoylation assay of control (si-non) and S1R-silenced (si-S1R) FAD NPCs detected lower level of *pal*APP on S1R silencing (ABE assay). Lower panel: conditioned media (CM) from control (si-non) and S1R-silenced (si-S1R) cells showed reduction of soluble sAPPβ (sAPPβ) level but not that of total sAPP (sAPPtot).

(B) Quantitative analyses of *pal*APP or sAPPβ levels from si-non and si-S1R cells. *pal*APP levels were normalized with total APP level (*pal*APP/$APP_{tot}$) and sAPPβ levels were normalized with total sAPP level (sAPPβ/$sAPP_{tot}$). We used ImageJ analysis and expressed the data as fold ± SEM (n = 3, *p < 0.01).

(C) ABE palmitoylation assay from FAD NPCs demonstrated increase or decrease of palmitoylated sAPPβ (*pal*-sAPPβ) release from cells treated with PRE-084 (PRE) or NE-100 (NE), respectively, as compared to untreated (veh) cells (ABE IB:anti-sAPPβ). Total

sAPPβ (sAPPβ), sAPP ($sAPP_{tot}$,) and sAPPα (sAPPα) were detected in the conditioned media (CM, IB:anti-sAPPβ, IB:22C11 and IB: anti-sAPPα, respectively).
(D) Quantitation of *pal*-sAPPβ release compared to total sAPPβ release from untreated (veh), PRE-, or NE-treated cells. The data were represented as fold ± SEM (n = 4, **p < 0.01).

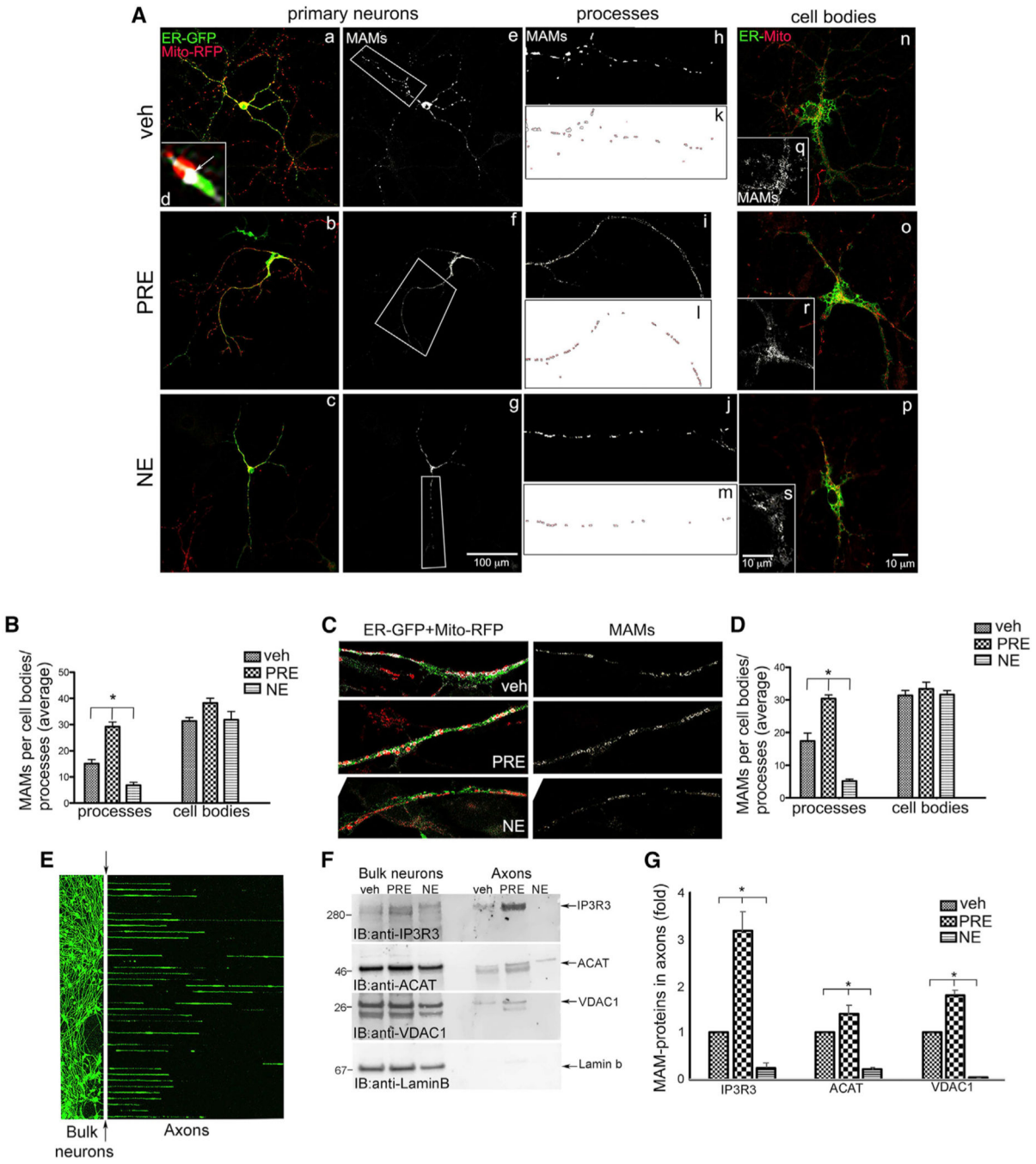


**Figure 6. Regulation of S1R-activity modulates MAMs in neuronal processes or axons without affecting MAMs in cell bodies or bulk neurons**

(A) Confocal microscopic images of primary neuronal cultures labeled with membrane permeable ER and mitochondria (mito) probes CellLight ER-GFP and CellLight mito-RFP in absence (veh) or presence of PRE-084 (PRE) or NE-100 (NE) (a–c). Inset (d): expanded representative image of MAMs at the contact sites between ER-GFP and mito-RFP (d, arrow). (e and f) Images of MAMs in neurons treated without (veh) or with PRE-084 (PRE) or NE-100 (NE). (h–j) Images of MAMs in neuronal processes (processes). (k–m) ImageJ images of MAMs in neuronal processes (processes). (n–p) Representative images of cell

bodies of primary neurons labeled with CellLight ER-GFP and CellLight mito-RFP (cell bodies). (q–s) Images of MAMs in cell bodies of neurons treated without (veh) or with PRE or NE.

(B) Quantitation of number of MAMs in neuronal processes and in cell bodies or primary neurons confirmed increased number of MAMs in neuronal processes after treatment without with PRE-084, and decreased number of MAMs in presence of NE-100 in comparison to control (veh) cells ($n = 25$, $^*p < 0.001$). No change in MAMs observed in the cell bodies of PRE- or NE-treated cells compared to control (veh) cells.

(C) Representative confocal microscopic images of neuronal processes of hNPCs pre-labeled with CellLight ER-GFP and CellLight mito-RFP (ER-GFP + mito- RFP) after treatment without (veh) or with PRE or NE. MAMs were identified by highlighting the ER-mito contact sites.

(D) Quantitation of MAMs from neuronal processes (processes) or cell bodies of hNPCs treated without (veh) or with PRE or NE ($n = 25$, $^*p < 0.001$).

(E) Schematic representation of microfluidic device manufactured to perform axotomy. The somal chambers and axonal chambers were linked with 195 capillaries. Cells seeded in the somal chambers generated axons along the capillaries, which were severed (arrow), and pure axons were obtained to extract axonal proteins.

(F) Confocal image of FAD hNPCs differentiated in a microfluidic chamber undergoing axotomy to separate bulk neurons from axons.

(G) Representative western blot images of bulk neurons and axons from control (veh), PRE- or NE-treated cells with indicated antibodies ($n = 3$, $^*p < 0.01$).

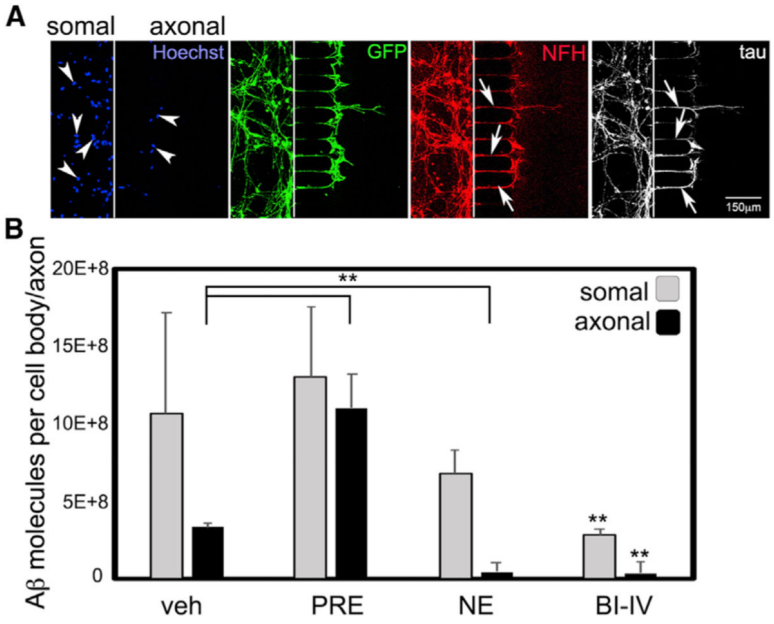


**Figure 7. Activation of S1R increases axonal $A\beta_{40}$ release from FAD hNPCs in 3-D neural cell cultures**

(A) Confocal microscopy of FAD hNPCs seeded in a Matrigel 3-D matrix on the somal chambers of microfluidic devices to develop axons along the capillaries (arrows). Hoechst (blue) labeled nuclei in the somal chamber, indicating cell bodies. GFP signals (green) showed cell morphology. Antibodies against axonal markers neurofilament H (NFH)-labeled (red) or tau (tau)-labeled (white) axons in axonal chambers.

(B) Aβ ELISA of conditioned media isolated from axonal chambers of the microfluidic devices undergoing a fluidic separation confirmed increased or decreased number of $A\beta_{40}$ molecules per axon after treatment with PRE-084 (PRE) or NE-100 (NE), respectively. Number of Aβ calculated by measuring $A\beta_{40}$ (in pM) levels in the conditioned media. Although PRE-treatment increased number of $A\beta_{40}$-release from axons by ~3-fold, NE-treatment decreased axonal $A\beta_{40}$-release to undetectable level. No significant changes in the number of $A\beta_{40}$ molecules released per cell body were detected after PRE- or NE-treatment. Treatment with BACE-inhibitor IV (BI-IV) reduced both somal and axonal $A\beta_{40}$ levels, as expected. Error bars indicated SEM from three independent experiments (**$p < 0.01$).

## KEY RESOURCES TABLE

| REAGENT or RESOURCE | SOURCE | IDENTIFIER |
|---|---|---|
| Antibodies | | |
| 22C11 (anti-APP N terminus) | Sigma-Millipore | Cat#MAB348, RRID: AB_2056583 |
| anti-s APP beta | IBL International | Cat#10321, RRID: AB_1630822 |
| anti-Sigma Receptor Antibody (B-5) (Mouse) | Santa Cruz | Cat#sc-137075, RRID: AB_2285870 |
| Purified Mouse anti-IP3R3 | BD Transduction Laboratories | Cat#610312, RRID: AB_397704 |
| anti-SOAT-1/ACAT-1 Polyclonal (Rabbit) | Cayman Chemical | Cat#100028, RRID: AB_327803 |
| Purified Mouse Anti-Flotillin-1 | BD Transduction Laboratories | Cat#610820, RRID: AB_398140 |
| anti-MAP2 (Rabbit) | Cell Signaling Technologies | Cat#4542, RRID: AB_10693782 |
| Anti-Grp75 antibody | Abcam | Cat# ab129201, RRID:AB_11141817 |
| Anti-Neurofilament heavy polypeptide antibody | Abcam | Cat#ab8135, RRID: AB_304560 |
| anti-Tau | Cell Signaling Technologies | Cat#A0024, RRID: AB_10013724 |
| anti-GAPDH | Life Technologies | Cat#MA5-15738-D680, RRID: AB_2537657 |
| anti- beta2 Adrenergic Receptor (Rabbit) | Abcam | Cat#ab176490, RRID: AB_2861265 |
| anti-Transferrin Receptor (Rabbit) | Abcam | Cat#ab84036, RRID: AB_10673794 |
| Anti-GRP94 (C-terminal) (Rabbit) | Sigma | Cat#G4420, RRID: AB_477017 |
| Anti-VDAC1 / Porin antibody [EPR10852(B)] (Rabbit) | Abcam | Cat#ab154856, RRID: AB_2687466 |
| anti-Laminb1 | Abcam | Cat#ab65986, RRID: AB_1140888 |
| Alexa Fluor 488 and 568 secondary antibody | Life Technologies | Cat#A32723, RRID: AB_2633275; A32731, RRID: AB_2633280; A-11011, RRID: AB_143157; A-11004, RRID: AB_2534072; A-11041, RRID: AB_2534098 |
| HRP conjugate secondary antibody | Life Technologies | Cat#G-21040, RRID: AB_2536527; G-21234, RRID: AB_2536530 |
| Anti-Cytochrome C antibody [7H8.2C12] (mouse) | Abcam | Cat#ab13575, RRID: AB_300470 |
| Anti-Tamara | Invitrogen, Thermo Fisher | Cat#MA1-041, RRID: AB_2536728 |
| Anti-GFP (chicken) | Abcam | Cat#ab13970, RRID: AB_300798 |
| C66 (Anti-APP C terminus) | In-house | https://www.ncbi.nlm.nih.gov/pmc/articles/PMC3718372/ |
| DMEM/F12 with L-glutamine | GIBCO/Thermo fisher | Cat#11320-033 |
| B-27 Supplement (50X), serum free | GIBCO/Thermo fisher | Cat#17504044 |
| bFGF | R&D System | Cat#233-FB |
| EGF | Sigma Aldrich | Cat#92090408 |
| Penicillin/Streptomycin/Amphotericin B | Lonza | Cat#17-745E |
| StemPro Accutase | GIBCO | Cat#2023-01-30 |
| DMEM 4.5 g/L Glucose w/o L-Gln w/Phenol Red | Lonza | Cat#BE12-614F |
| Alkylene Palmitic acid (Alkyl C-16) | Invitrogen | Cat#C10265 |
| Click-it reagents, alkyne-Tetramethylrhodamine | Invitrogen | Cat#C10269, T10183 |
| PRE-+B34:C48084 hydrochoride | Tocris Bioscience | Cas#138847-85-5 Batch# 2A/222270 |
| NE-100 | Sigma Aldrich | Cat#SML0631 |
| Cerulenin | Sigma Aldrich | Cat#P2607 |

| REAGENT or RESOURCE | SOURCE | IDENTIFIER |
|---|---|---|
| EZ-Link Sulfo-NHS-SS-Biotin | Thermo Scientific | Cat#21335 |
| BACE1 inhibitor IV | (BACE1-IV) Calbiochem | Cat#565788 |
| CellLight ER-GFP BacMam 2.0 | Thermo fisher | Cat#C10590 |
| CellLigh Mitochondria-RFP BacMam 2.0 | Thermo fisher | Cat#C10601 |
| Hoechst 3342 | Thermo fisher | Cat#H3570 |
| Lubrol | Calbiochem | Cat#205528 |
| Percol | Sigma Aldrich | Cat#P4937 |
| Triton X-100 | Sigma Aldrich | Cat#T8787 |
| n-Octylglucoside | Sigma Aldrich | Cat#10634425001 |
| Cyclohexamide | Sigma Aldrich | Cat#C7698 |
| Lipofectamine 2000 Transfection Reagent | Invitrogen | Cat#11668019 |
| NuPAGE 4-12% Bis-Tris gel | Invitrogen | Cat#NP0321BOX |
| Matrigel Basement Membrane Matrix | Corning | Cat#356234 |
| Critical commercial assays | | |
| CAPTUREome S-Palmitoylation Protein mini kit | Badrilla | Cat#K010-310 |
| Human/Rat beta amyloid (40) ELISA Kit | Wako | Cat#294-62501 |
| Human/Rat beta amyloid (42) ELISA Kit | Wako | Cat#290-62601 |
| Amexa mouse Neuron Ncleofactor kit | Lonza | Cat#VPG-1001 |
| Cyto Tox-One assay | Promega | Cat#G3582 |
| Software | | |
| ImageJ Software | ImageJ 1.53a | N/A |
| Photoshop | Adobe Photoshop CC 20.0.10 | N/A |
| Graphpad Prism | Prisom 9, version 9.0.2 | N/A |
| MS Excel | Microsoft Excel, version 16.30 | N/A |
| Oligonucleotides | | |
| split GFP constructs (provide sequence for both ER and mito) | Dr. Chao Tong, Professor, Life Sciences Institute, Zhejiang University, China | N/A |
| SMART pool siRNA against sigma-1 receprot (S1R) | Dharmacon, Inc. | N/A |
| Other/devices | | |
| XonaChip 450um | Xona Microfluidics | Cat#XC450 |
| XonaChip 150um | Xona Microfluidics | Cat#XC150 |
| Microfluidic Chips (5 × 8 × 450 um) (H x W x L) | In-house (designed by M.J.) | N/A |